5-2011

Dynamics of Mushy Layers on a Finite Domain

Nicholas Ray Gewecke
ngewecke@utk.edu

To the Graduate Council:

I am submitting herewith a dissertation written by Nicholas Ray Gewecke entitled "Dynamics of Mushy Layers on a Finite Domain." I have examined the final electronic copy of this dissertation for form and content and recommend that it be accepted in partial fulfillment of the requirements for the degree of Doctor of Philosophy, with a major in Mathematics.

Timothy P. Schulze, Major Professor

We have read this dissertation and recommend its acceptance:

Vasilios Alexiades, Yanfei Gao, Suzanne Lenhart

Accepted for the Council:
Dixie L. Thompson

Vice Provost and Dean of the Graduate School

(Original signatures are on file with official student records.)

Dynamics of Mushy Layers on a Finite Domain

A Dissertation
Presented for the
Doctor of Philosophy
Degree
The University of Tennessee, Knoxville

Nicholas Ray Gewecke
May 2011

Dedication

I dedicate this dissertation to my wife, Anna, and to my parents, Allen and Nancy Gewecke. Their extensive love, support, and encouragement are deeply appreciated.

Acknowledgements

Abstract

Mushy layers are regions of intermixed liquid and solid which can arise during the solidification of binary alloys, generally consisting of dendritic solids with solute-rich liquid in the interstices. They occur due to an instability resulting from the buildup of rejected solute along the solidification front. Liquid ahead of the front becomes supercooled, so disturbances to the interface grow more rapidly than the interface itself. A simple experiment has a tank filled with a uniform solution at uniform temperature being placed upon a cold surface. Early on, a small solid layer forms at the bottom capped by a rapidly advancing mushy layer. Typical modeling efforts have made at least one of two assumptions, that the tank is of infinite depth or that the diffusion of solute is negligible. This dissertation investigates the finite-domain problem in the presence of solute diffusion, highlighting new interfacial dynamics and other behaviors that arise in this case.

Contents

List of Tables

List of Figures

Chapter 1

Introduction

1.1 Preliminaries

Solidification of alloys is a process which occurs both in industrial settings and the natural world. The formation of sea ice and the cooling of magma chambers both serve as natural examples. In industry, solidification of alloys is present in semiconductor manufacturing. Metallurgical examples are also very common, for example bronze, brass, and steel. The low melting point of mercury alloys lead to the use of amalgam for dental fillings.

In this dissertation, we address binary alloys, which consist of two components. While there are many metallurgical examples, including common alloys such as bronze (copper and tin), brass (copper and zinc), and steel (iron and carbon), binary alloys do not need to be metallic. For example, a simple salt solution (sodium chloride and water) is a binary alloy. Throughout this dissertation, we will approximate a sodium nitrate solution. However, many experiments investigating issues associated with solidification of binary alloys utilize an ammonium chloride solution. In common language, alloys are typically solid and solutions are typically liquid, but both terms may refer to substances in either phase. Throughout this dissertation, we use this more general definition.

A fairly simple experimental arrangement is to take a tank filled with a uniformly-mixed solution which is at some uniform temperature and place it upon a cold surface. The top of the tank is held at a fixed warm temperature, the bottom is held at a fixed cold temperature, and the sides are insulated. One of two phenomena may occur. The first is that a solid will grow from the bottom with a planar solid-liquid interface. The second is that a solid layer will grow from the bottom, but with a very convoluted solid-liquid interface. In fact, this convoluted interface may be difficult to detect with the human eye, as the solid forms dendritic structures that are intermixed with liquid. Frequently, a completely solid layer and a completely liquid layer would be perceived with a third layer in the middle. At smaller scales, one can see that this middle layer is made up of solid dendrites surrounded by liquid. This layer has come to be called a mushy layer, mush, or mushy zone. A schematic of this arrangement is given in figure 1.1(a), with the representative profile for the fraction of the mushy layer which is solid shown in figure 1.1(b)) and representative temperature and concentration profiles on the full domain shown in figure 1.1(c). The temperature is increasing throughout the domain, fixed at the cold temperature T_B at the bottom of the tank and a warm temperature T_H at the top of the tank, which is also the initial temperature throughout the tank. This experimental arrangement forms the basis for our model.
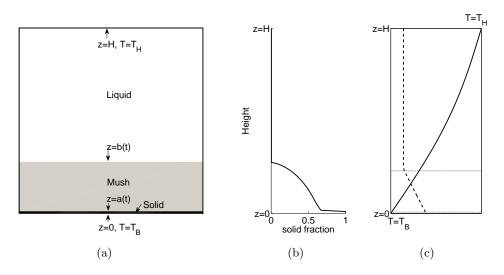
Figure 1.1: A finite-depth tank filled with a uniformly mixed solution is placed on a cold boundary. Two time-dependent interfaces form, separating the domain into three regions as shown in (a): a thin solid layer at the bottom (not visible on the scale shown), mush in the middle (grey), and liquid at the top (white). In (b), we see the corresponding curve for the solid fraction, which decreases from the solid-mush interface to the mush-liquid interface. In (c), representative temperature (solid, varying from $T = T_B$ to $T = T_H$) and concentration (dashed) curves are shown, with interface positions shown as horizontal lines.
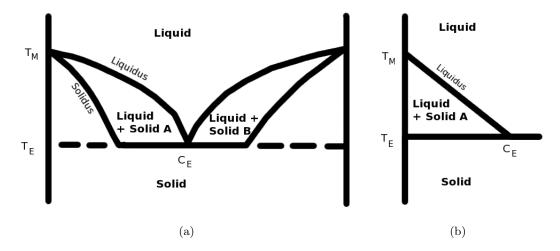
Figure 1.2: The full phase diagram for a binary system is given in (a), whereas the simplified phase diagram that will be used in our analyses is given in (b).

Phase transitions in binary alloys are more complicated than the transitions in pure materials. A pure material, at a fixed pressure value, has a particular freezing temperature, below which it will solidify and above which it is liquid. Binary alloys, on the other hand, have variable freezing temperatures dependent upon the concentration. Full and simplified phase diagrams for a binary alloy are demonstrated in figure 1.2. The liquidus temperature $T_L(C)$ is the temperature at which an alloy at concentration C will begin to solidify, and the solidus temperature $T_S(C)$ is the temperature at which the alloy will begin to melt. The full phase diagram, given in figure 1.2(a), describes the equilibrium configuration of an alloy at temperature T and concentration C. If the associated point falls in the liquid or solid regions, then the alloy will be liquid or solid at equilibrium. If the associated point falls into the "Liquid + Solid A" region, then the state at equilibrium will contain both liquid and solid. If a line is drawn across the left half of the phase diagram at the temperature T of the alloy, then the concentration value along the solidus curve is the concentration C_s that will appear in the solid portion of the alloy at equilibrium, and the concentration value along the liquidus curve is the concentration C_L that will appear in the liquid portion of the alloy. The fraction of the alloy in the liquid phase is given by the lever rule,

$$\chi = \frac{C - C_S}{C_L - C_S}.$$

The eutectic concentration C_E is the concentration value at which the freezing temperature is minimized, and corresponds to the eutectic temperature T_E. Regardless of concentration, if $T < T_E$, then the alloy will be completely solid at equilibrium. In other words, the eutectic temperature is the lowest possible melting temperature of the alloy.

We will utilize a simplified phase diagram, as in figure 1.2(b). This is representative of phase diagrams for many aqueous solutions, which are commonly used in experiments due to their transparency. Here, the liquidus curve is linear, so that the liquidus temperature is given by

$$T_L(C) = T_M - \Gamma C, \tag{1.1}$$

3

where T_M is the melting temperature of the pure material and Γ is the slope of the liquidus curve. The solidus curve is now vertical, reflecting an assumption of complete solute rejection. One example of this phase diagram is related to sea ice, which is fresh even though it is the result of a solidifying brine. During the evolution of a mushy layer, it is typically assumed that the dendrites grow or melt in order to maintain local thermal equilibrium, which is represented by assuming that the temperature and concentration within the mushy layer obey the liquidus relationship. In a more general situation where solute is not completely rejected, then the liquidus relationship would dictate the concentration of solute in the liquid phase of the mushy layer and the solidus relationship would dictate the concentration of solute within the dendrites.

The linear stability of a planar solid-liquid interface during solidification of binary alloys was studied by Mullins and Sekerka (1964). An arbitrary perturbation to the interface is described by its Fourier expansion, and the interface is stable if all of the Fourier modes decay with time. Under the assumptions of negligible latent heat, uniform thermal properties, and negligible surface energy, which will be used throughout in this dissertation, the condition for instability identified by Mullins and Sekerka (1964) reduces to the presence of supercooling in the liquid near the interface. In the case of binary alloys, the liquid is supercooled if the temperature is below the liquidus temperature of the local concentration. It had previously been thought, as in Rutter and Chalmers (1953), that the presence of supercooling was generally the condition for instability, since supercooling leads to instability during solidification of a pure melt, as described in Langer (1980). An argument for the utilization of this simplified condition in more general circumstances is given by Worster (1986). Additionally, Wilson et al. (1982) argued, based on equilibrium dynamics, that a mushy layer should be predicted to occur whenever supercooling is present at the interface. For a one-dimensional setting, supercooling at the interface can be expressed by the inequality

$$\left(\frac{\partial T}{\partial z}\right)_{h^+} < -\Gamma \left(\frac{\partial C}{\partial z}\right)_{h^+},$$

where $z = h(t)$ is the location of the solid-liquid interface. The notation $(\cdot)_{h^+}$ indicates that the quantity is evaluated as a limit from above, for example,

$$\left(\frac{\partial T}{\partial z}\right)_{h^+} = \lim_{z \to h^+} \frac{\partial T}{\partial z}.$$

This can also be thought of as the gradient of the quantity ahead of the interface, which would be on the liquid side of the interface in the present case.

The physical interpretation for linear instability in the presence of supercooling is as follows. As the alloy solidifies, rejected solute accumulates in the liquid immediately adjacent to the front. Higher concentrations of solute suppress the freezing temperature; the idea behind spreading salt on icy roads in order to encourage melting of the ice is a result of this property. Perturbations to the interface which protrude into the liquid will encounter reduced solute concentrations. If supercooling occurs, then the temperature along such a perturbation will be below the freezing temperature, so the perturbation will grow into the supercooled region. As a result, the perturbations grow more rapidly, so the interface is unstable.

The solid-liquid interface within a mushy layer is very convoluted. Tracking such a complicated interface is a difficult proposition, so other methods have been developed to

model mushy layers. The most common techniques treat the mushy layer as a continuum. The method utilized in this dissertation is the approach taken by Worster (1986), where the mushy layer is essentially treated as a third phase, along with the liquid and solid phases. This results in the problem being split into three domains, one each for solid, mush, and liquid. The properties in the mushy layer vary with the local liquid fraction, which is determined by averaging over a scale that is larger than the pore size.

Another approach is to use thermodynamic principles on the whole domain. One example is an enthalpy formulation. Wilson et al. (1984) formulated such a model for binary alloy solidification, with one cold boundary and one insulated boundary, where solid and liquid regions could be identified along with a possible intermediate zone. Le Bars and Worster (2006) formulated a two-dimensional model with a cold boundary opposite a warm boundary and two insulated side boundaries. This model includes flow terms, so that convective effects can be captured. Other authors, such as Hills et al. (1983), have formulated models using mixture theory.

While not addressed by the models presented in this dissertation, effects related to flow are often of great interest. Convective instabilities, which will be discussed later in this section, are of great interest. The mushy layer is a porous medium, so Darcy's equation is typically used. The permeability in the mushy layer is assumed to be some function of the local solid fraction. Additionally, a Boussinesq approximation is utilized, restricting density variations to the buoyancy terms only.

There are other experimental arrangements similar to the one utilized in this dissertation. A simple variation is to assume that the upper boundary is insulated, rather than held at a fixed temperature. This permits the mushy layer to grow to the top of the tank, and may lead to complete solidification if the cold boundary is sufficiently cold. This particular approach has been utilized by Huppert and Worster (1985) for a sodium nitrate solution and Aitta et al. (2001) for a ternary alloy. The use of a cold upper boundary and an insulated lower boundary has proved useful in experiments analyzing the growth of sea ice and cooling of magma chambers. A series of papers (Kerr et al. (1990a), Kerr et al. (1990b), and Kerr et al. (1990c)) investigated the evolution of various aqueous solutions in such experiments. Wettlaufer et al. (1997b) used this arrangement with a sodium chloride solution and with sea water to study the growth of sea ice, with further exploration of convective effects in Wettlaufer et al. (1997a).

A related process that has received considerable attention is the case where a melt is translated through a specified temperature field. This is variously called directional solidification or continuous casting of alloys. A major focus of related theoretical research relates to the stability of the steady states, under the assumption of an infinite domain. A sketch of this configuration is shown in figure 1.3. If the cold temperature applied is below the eutectic then a eutectic solid grows capped by a mushy layer, with liquid melt extending into the farfield. Such models exhibit a steady state, where the solid-mush and mush-liquid interfaces advance upward at a rate equal to the rate that the melt is being translated through the temperature field, so that an observer in the laboratory sees a fixed position of the interfaces. Aspects of this process have been studied theoretically by many authors, including Langer (1980), Worster (1992), Emms and Fowler (1994), Schulze and Worster (1999), Chung and Chen (2000), Roper et al. (2007), and Roper et al. (2008).

Comparisons between theory and experiment frequently address the temperature and concentration profiles along with the interface positions, but another important aspect is the solid fraction within the mushy layer. In the context of sea ice, there is also interest in
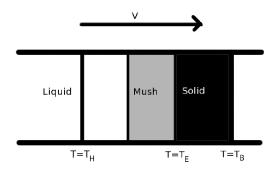
Figure 1.3: During directional solidification, the melt is translated through a specified temperature field. In this schematic, the melt is being translated to the right at velocity V past a hot contact at temperature $T = T_H$ and a cold contact at temperature $T = T_B$. At steady state, a solid layer and a mushy layer appear as shown.

measuring devices that can be deployed in the environment to collect data. Experiments which utilize conduction of electricity have exhibited good agreement with the solid fraction values determined from mathematical models. One experiment in the case of cooling from below, developed by Shirtcliffe et al. (1991), uses individual thin platinum wires placed at varying heights with a large carbon block above the wires. Each wire in combination with the carbon block formed a conductivity cell. Since pure ice is a good insulator, the solid fraction near each wire could be calculated based on the conductivity of the liquid and the resistance of the cell. A concern with these experiments is that the crystals may grow preferentially along the wires, which would increase the observed solid fraction, but Notz et al. (2005) assert that the effect is minimal. Another experiment developed by Shirtcliffe and Kerr (1992) for cooling from below, and later adapted for cooling from above by Notz et al. (2005), uses pairs of wires at each height as a conductivity cell, rather than a single wire with a distant carbon block.

Instabilities in the growth of mushy layers are also of great interest. Convective instabilities can occur within the mush or in a boundary layer near the mush-liquid interface. Typically, these instabilities are expected in the case of cooling from below if the density of the liquid decreases as the concentration increases. If these instabilities occur within the mushy layer, then certain defects called chimneys appear (see Fowler (1985)). These chimneys are channels in the mush with zero solid fraction. A summary and review of relevant literature is contained in Worster (1997). Worster and Wettlaufer (1997) compared theoretical and experimental results with regards to the formation of sea ice, where solidification occurs from above.

A variety of experiments have been performed examining chimney formation. Sample and Hellawell (1984), Chen and Chen (1991), and Chen (1995) examined the case of solidification from below with an insulated upper boundary. The study of Sample and Hellawell (1984) also studied the effects of rotating the mold during solidification. Solomon and Hartley (1998) tested the case of solidification from below with a fixed temperature at the upper boundary, which relates to the study in this dissertation. These studies all identified a finger convection associated with the compositional boundary layer near the mush-liquid interface, which preceded the plume convection in the mushy layer. The finger convection

is a fine scale convection, while the plume convection is on a larger scale. This plume convection causes the chimneys to form. Another case of solidification from above was studied by Aussillous et al. (2006) using a sucrose solution. This experiment is notable because the chimneys formed were branched and did not completely penetrate the mushy layer, due to high viscosity of the sucrose at low temperature near the top of the mush.

Many theoretical studies of convective instabilities utilize the assumption that the solid-mush and mush-liquid interfaces advance with constant velocity V, which reflects the case of directional solidification. Other common assumptions in these studies are that solute diffusivity is negligible and that the mush-liquid interface is rigid and impermeable. Studies using these assumptions include Worster (1992) and Emms and Fowler (1994). Chung and Chen (2000) allowed the interface to be permeable, and Schulze and Worster (1999) and Roper et al. (2008) additionally allowed the interface to be deformable. The earlier studies exhibited chimney which initiated deep within the mush, whereas these later studies indicate that chimneys initiate near the mush-liquid interface owing to the permeability of the interface. Convection caused by sidewall heat loss has been studied by Roper et al. (2007), with a hypothesis that chimneys would form near the sidewalls due to upflow being greatest there, although no stability analysis was performed.

Throughout this dissertation, we will utilize an assumption of negligible latent heat. This assumption has commonly been used in the study of mushy zones. For example, it is part of the frozen temperature approximation, which is understood to be a collection of three assumptions (see Davis (2001)): thermal diffusion is much faster than solute diffusion; latent heat is negligible; and the temperature profile is given by its steady state. The frozen temperature approximation was used by Langer (1980) to study mushy layers appearing during directional solidification of binary alloys. Studies often show that the influence of latent heat is rather weak. For example, Kerr et al. (1990a) investigated the effects of varying the Stefan number, which is equivalent to varying latent heat, when solidifying an alloy from above. The case of negligible latent heat (zero Stefan number) was included in that study. The most visible effect of increasing the Stefan number is that solidification is slowed.

A critical issue in this dissertation is the treatment of a variety of conditions at the solid-mush and mush-liquid interfaces. This idea has arisen before, as Schulze and Worster (2005) consider boundary conditions along mush-liquid interfaces in the absence of solute diffusion, but in a crystal-pulling arrangement with a solid phase that moves steadily relative to the liquid phase. That study classifies the interface conditions into four different scenarios based upon the velocity of the solid phase, the velocity of the mush-liquid interface, and the velocity of the liquid. While the arrangement is different, the classification of the interface conditions still depends upon different velocities that arise in the problem.

Numerical calculations throughout this dissertation will utilize values given in Set I of Table 1 of Worster (1986), roughly approximating a 14% sodium nitrate solution. While the values in Set II more accurately model this solution, incorporating different thermal properties between the solid and liquid phases, the values in Set I serve as an approximation including the assumption of uniform thermal properties. We provide in Table 1.1 the values needed for our study, with a modification to the liquidus slope value, reflecting our use of a mass fraction for concentration as opposed to a mass percentage. Temperatures are in degrees Celsius, with $T_M = 0$ being the melting temperature of pure water. The eutectic point is assumed to be at $T_E = -20$ and $C_E = 0.5$. This is surely not the true eutectic point but will still serve to illustrate the qualitative behaviors when eutectic effects are accounted

Table 1.1: Parameters approximating a 14% sodium nitrate solution.

Parameter	Symbol	Value	Units
Liquidus slope	Γ	40	$^\circ$ C
Solute diffusivity	D	1.0×10^{-5}	$\mathrm{cm^2 s^{-1}}$
Thermal diffusivity	κ	1.3×10^{-3}	$\mathrm{cm^2 s^{-1}}$

for.

1.2 Contributions

The research presented in this dissertation includes results reported in Gewecke and Schulze (2011), as well as results that have not yet been reported. In particular, the majority of Chapter 3 and Appendix A provides the results of Gewecke and Schulze (2011) along with additional discussion.

Chapter 2 contains many results pertaining to the infinite-domain problems that are special cases of the models used by Worster (1986) and Anderson (2003). Each of those previous studies included more general results than those included in this dissertation. Section 2.4 contains novel results, identifying the transition point between the cases studied by those authors.

Chapters 3 and 4 contain a variety of new results for mushy layers on a finite domain. The role of solute diffusion leads to changes through time in the interfacial conditions at the solid-mush and mush-liquid interfaces. Previous studies provide reasonable approximations of the behaviors over the thermal diffusivity timescale. In addition, the diffusive effects ultimately lead to elimination of the mushy layer on the solute diffusivity timescale, which is much slower.

The main contribution of this dissertation is the identification of long-term behaviors in the finite-domain case that have appear when solute diffusion is present. The eventual disappearance of the mushy layer does not occur in a semi-infinite domain or when solute diffusion is assumed to be negligible. In addition, when eutectic effects are considered, this work demonstrates that the solid layer at the bottom of the tank has a variable concentration, which is not observed under those same common assumptions.

1.3 Applications and Broader Impacts

Various studies address the evolution of mushy layers on an infinite domain. The evolution of sea ice or the cooling of magma chambers occur in large spatial domains, but they are still finite domains. On these geologic spatial domains, the timescales for thermal and solute diffusion become very large. However, on geologic timescales, the effects of solute diffusion on finite domains highlighted by this research could have important consequences in these applications.

1.4 Dissertation Organization

In Chapter 2, we discuss solidification of dilute binary alloys on an infinite domain. The related problems admit similarity solutions, and these solutions are presented under the

assumptions utilized throughout this dissertation. Finally, we develop methods to identify when a mushy layer first appears and when the solid-mush interface conditions change.

In Chapter 3, we examine the dynamics of a mushy layer on a finite domain when eutectic effects are not present. Applicable mush-liquid interface conditions are identified, and associated with a condition on the interface velocity. The method of characteristics is applied in the mushy layer, which permits the development of a numerical scheme to solve the mushy layer problem on the finite domain.

In Chapter 4, we examine the dynamics of a mushy layer on a finite domain when eutectic effects are included. In addition to the issues addressed in Chapter 3, we identify the issues that arise at the solid-mush interface. After modifying our numerical scheme to account for the possibility of a eutectic solid-mush front, in addition to a diffusion-controlled solid-mush front, we are able to demonstrate numerically that both types of solid-mush front can occur. Furthermore, we demonstrate variability of solute concentration in the solid which forms in this case.

Finally, in Chapter 5, we identify related questions whose answers would generalize the results in this dissertation.

Chapter 2

Solidification in a semi-infinite domain

In this chapter, we study solidification from a cold lower boundary under the common assumption of a semi-infinite domain. The models presented in this chapter admit similarity solutions. To determine similarity solutions, a particular relationship between the spatial and temporal variables is used which transforms the system of partial differential equations into a system of ordinary differential equations. For the mushy layer models, there are two cases for the solid-mush interface to consider. One case is a diffusion-controlled interface and the second is a eutectic interface. This issue is accounted for in the models of Fowler (1985) and Emms and Fowler (1994), with little discussion. In terms of the similarity solution, only one of these two cases will apply for a given set of parameters. If all other parameters are fixed, there is a critical temperature at the base of the tank where the change between the cases occurs. This critical temperature will be referred to as a switching temperature. There is also a switching temperature for the transition from the presence of a solid-liquid interface to the presence of a mushy layer.

For the numerical schemes implemented on a finite domain in Chapters 3 and 4, we will incorporate the similarity solutions for the semi-infinite domain as a short-time approximation. Additionally, the switching temperature presented in Section 2.4 will inform which similarity solution to apply for this approximation. Worster (1986) solves the Stefan problem for binary alloys freezing from a cold planar surface, as highlighted in Section 2.1, and presents a model with a mushy layer. This mushy layer model, which incorporates a diffusion-controlled solid-mush interface, is presented in Section 2.2, along with a binary alloy analogue of the ternary alloy model presented by Anderson (2003), which incorporates a eutectic solid-mush interface. These mushy layer models treat the mushy layer as a third phase, where the properties vary with the liquid fraction. The model then has three domains, one each for the solid, mush, and liquid. The models will be presented with latent heat, but we will ultimately incorporate an assumption of negligible latent heat which is important in the analysis in Chapters 3 and 4.

2.1   Binary Stefan problem

The Stefan problem for a binary alloy is similar to the well-studied Stefan problem for pure materials. Worster (1986) describes the model for binary alloys in a more general form than

presented here, as the present analysis utilizes an assumption of uniform thermal properties in each phase.

Initially, the domain $z \geq 0$ is filled with a liquid binary alloy with uniform temperature T_∞ and concentration C_0. Note that the concentration C is a mass fraction of the solute within the liquid phase as opposed to the weight percentage used in Worster (1986), but the difference between the two is simply a factor of 100. The restrictions on the initial conditions are that $0 \leq C_0 < C_E$ and $T_\infty > T_L(C_0)$, where $T = T_L(C_0)$ is the temperature on the liquidus curve associated with $C = C_0$ given by (1.1). The initial conditions are therefore

$$T(z, 0) = T_\infty, \tag{2.1a}$$

$$C(z, 0) = C_0. \tag{2.1b}$$

For $t > 0$, a solid region grows from the lower boundary. In the farfield $z \to \infty$,

$$T \to T_\infty, \tag{2.2a}$$

$$C \to C_0. \tag{2.2b}$$

In the liquid region $z > h(t)$ heat and solute diffuse, so

$$\frac{\partial T}{\partial t} = \kappa \frac{\partial^2 T}{\partial z^2}, \tag{2.3a}$$

$$\frac{\partial C}{\partial t} = D \frac{\partial^2 C}{\partial z^2}, \tag{2.3b}$$

where κ and D are the thermal and solutal diffusivities, respectively.

At the solid-liquid interface $z = h(t)$,

$$\frac{L}{c_p} \dot{h} = \kappa \left(\frac{\partial T}{\partial z} \right)_{h^-} - \kappa \left(\frac{\partial T}{\partial z} \right)_{h^+}, \tag{2.4a}$$

$$C_{h^+} \dot{h} = -D \left(\frac{\partial C}{\partial z} \right)_{h^+}, \tag{2.4b}$$

$$[T]_-^+ = 0, \tag{2.4c}$$

$$T_h = T_M - \Gamma C_{h^+}, \tag{2.4d}$$

where $[\cdot]_-^+$ denotes the jump of the quantity across the interface, T_M is the melting temperature of the pure liquid, L is the latent heat, c_p is the specific heat, and Γ is the slope of the liquidus curve. Additionally, $(\cdot)_{h^+}$ indicates the value of the quantity computed as a limit from above, which is the value of the quantity on the liquid side of the interface. The first condition is a Stefan condition, balancing heat flux with the release of latent heat due to solidification. The second condition balances solute flux with the solute rejected during solidification. The condition (2.4d) indicates that the temperature at the interface is the liquidus temperature.

There is no solute diffusion within the solid, but the diffusion of heat is still present. Hence, in the solid region $0 < z < h(t)$,

$$\frac{\partial T}{\partial t} = \kappa \frac{\partial^2 T}{\partial z^2}. \tag{2.5}$$

Since solute is completely rejected, the mass fraction of solute in the solid phase is $\mathscr{C} = 0$.

At the lower boundary $z = 0$, the temperature is fixed at a cold temperature $T_B < T_L(C_0)$, so

$$T(0, t) = T_B. \tag{2.6}$$

This model admits a similarity solution, which will be discussed in Section 2.3.

2.2 Mushy layer problems

The model in Section 2.1 applies until an instability occurs at the interface leading to the formation of a mushy layer. It is well understood that supercooling ahead of the interface leads to such instability, and this can be expressed by the condition

$$\left(\frac{\partial T}{\partial z}\right)_{h^+} < -\Gamma \left(\frac{\partial C}{\partial z}\right)_{h^+}. \tag{2.7}$$

For the mushy layer model, there is a solid region which grows from the lower boundary, then a mushy layer, then a liquid region which extends into the farfield. Depending upon the parameters in the system, there are two different solid-mush interfaces which can appear. One of these is a eutectic interface, which is dictated by the advance of the $T = T_E$ isotherm. The other is diffusion-controlled interface, which will also be referred to as a noneutectic interface, whose advance is restricted by the diffusion of rejected solute away from the interface. The first interface type appears in a model for ternary alloy solidification with $T_B \ll T_E$ studied by Anderson (2003). The second interface type is studied in Worster (1986), which focused on the case $T_B \geq T_E$. Here, the model studied by Worster (1986) will be presented, followed by a discussion of the changes needed for the case of a eutectic solid-mush interface. In each case, we let $a(t)$ and $b(t)$ denote the solid-mush and mush-liquid interface positions, respectively.

The initial conditions for the mushy layer problem are the same as in the Stefan problem, with the entire domain $z > 0$ filled with a uniform solution at concentration C_0 and temperature $T_\infty > T_L(C_0)$, so

$$T(z, 0) = T_\infty, \tag{2.8a}$$

$$C(z, 0) = C_0. \tag{2.8b}$$

Similarly, the farfield $z \to \infty$ conditions remain unchanged,

$$T \to T_\infty, \tag{2.9a}$$

$$C \to C_0. \tag{2.9b}$$

In the liquid region $z > b(t)$,

$$\frac{\partial T}{\partial t} = \kappa \frac{\partial^2 T}{\partial z^2}, \tag{2.10a}$$

$$\frac{\partial C}{\partial t} = D \frac{\partial^2 C}{\partial z^2}. \tag{2.10b}$$

At the mush-liquid interface $z = b(t)$,

$$[T]_-^+ = 0, \tag{2.11a}$$

$$[C]_-^+ = 0, \tag{2.11b}$$

$$\frac{L}{c_p}(1 - \chi_b)\dot{b} = \kappa\left(\frac{\partial T}{\partial z}\right)_{b-} - \kappa\left(\frac{\partial T}{\partial z}\right)_{b+}, \tag{2.11c}$$

$$C_b(1 - \chi_b)\dot{b} = D\chi_b\left(\frac{\partial C}{\partial z}\right)_{b-} - D\left(\frac{\partial C}{\partial z}\right)_{b+}, \tag{2.11d}$$

$$\left(\frac{\partial T}{\partial z}\right)_{b+} = -\Gamma\left(\frac{\partial C}{\partial z}\right)_{b+}, \tag{2.11e}$$

where $\chi(z,t)$ denotes the liquid fraction. The condition of marginal equilibrium (2.11e) reflects the concept that the mushy layer grows sufficiently to relieve undercooling. That is, the mushy layer grows until the inequality (2.7) no longer holds at the interface. As shown below, the temperature and concentration within the mushy layer are tied together through the liquidus relationship (1.1). Combining this with the continuity of temperature and concentration at the mush-liquid interface, we find that

$$T_b = T_M - \Gamma C_b.$$

Inside the mushy layer $a(t) < z < b(t)$,

$$\frac{\partial T}{\partial t} = \kappa\frac{\partial^2 T}{\partial z^2} - \frac{L}{\rho c_p}\frac{\partial \chi}{\partial t}, \tag{2.12a}$$

$$\frac{\partial(\chi C)}{\partial t} = D\frac{\partial}{\partial z}\left(\chi\frac{\partial C}{\partial z}\right), \tag{2.12b}$$

$$T = T_M - \Gamma C, \tag{2.12c}$$

where ρ is the density of the liquid. The third equation reflects local thermodynamic equilibrium, which represents the assumption that the dendrites composing the mush grow or decay sufficiently to maintain the liquidus relationship.

At the solid-mush interface $z = a(t)$,

$$[T]_-^+ = 0, \tag{2.13a}$$

$$\frac{L}{c_p}\chi_a\dot{a} = \kappa\left(\frac{\partial T}{\partial z}\right)_{a-} - \kappa\left(\frac{\partial T}{\partial z}\right)_{a+}, \tag{2.13b}$$

$$C_{a+}\chi_a\dot{a} = -D\chi_a\left(\frac{\partial C}{\partial z}\right)_{a+}. \tag{2.13c}$$

In the solid $0 < z < a(t)$, heat diffuses but solute does not, so

$$\frac{\partial T}{\partial t} = \kappa\frac{\partial^2 T}{\partial z^2}, \tag{2.14a}$$

$$\frac{\partial \mathscr{C}}{\partial t} = 0, \tag{2.14b}$$

where $\mathscr{C}$ is the mass fraction of the solute in the solid phase. For the case of a noneutectic

solid-mush front, $\mathscr{C} = 0$ as no solute is being frozen into the solid. In the case of a eutectic solid-mush front, discussed below, $\mathscr{C} > 0$ is possible, and will be determined by a condition at the solid-mush interface.

At the lower boundary $z = 0$, for $t > 0$,

$$T = T_B. \tag{2.15}$$

The above assumes that a noneutectic solid-mush front appears. For sufficiently cold temperatures T_B at the lower boundary, the solid-mush front will be a eutectic front. In this case, the conditions given by (2.13a)-(2.13c) at the solid-mush interface $z = a(t)$ are replaced by the conditions

$$T = T_E, \tag{2.16a}$$

$$[T]_-^+ = 0, \tag{2.16b}$$

$$\frac{L}{c_p}\chi_a \dot{a} = \kappa \left(\frac{\partial T}{\partial z}\right)_{a^-} - \kappa \left(\frac{\partial T}{\partial z}\right)_{a^+}, \tag{2.16c}$$

$$\left(\mathscr{C}_{a^-} - C_{a^+}\chi_{a^+}\right)\dot{a} = D\chi_{a^+}\left(\frac{\partial C}{\partial z}\right)_{a^+}. \tag{2.16d}$$

Since the liquidus relationship (2.12c) holds in the mushy layer, the concentration on the mush side of the interface is

$$C_{a^+} = C_E.$$

The final condition describes the quantity of solute being frozen into the solid.

For problems like this, the number of boundary and interface conditions is very important. The temperature field is governed by the heat equation in each region, with a source term in the mushy layer. Since we have two interfaces, a lower boundary, and a farfield boundary, a total of six conditions are required for the temperature; two conditions are needed for each of the regions. At the two boundaries, the temperature is fixed, providing two of these conditions. The other four are the jump conditions for temperature and its gradient at the interfaces. Since the temperature and concentration in the mushy layer being tied together through the liquidus relationship (2.12c), we find the (2.12b) becomes an evolution equation for the liquid fraction. As a result, the concentration field is governed by the diffusion equation in the liquid region and the temperature field in the mushy layer, so only two boundary conditions are need to determine the concentration profile. The liquid fraction is governed in the mush by (2.12b), which is a first-order partial differential equation. As a result, it needs a single boundary condition. We also need an additional condition to determine each of the two interfaces. For the case of a eutectic front, we also need a condition for $\mathscr{C}$. Hence, we need eleven combined boundary and interface conditions for a diffusion-controlled front, and twelve for a eutectic front. Our models include the needed number of conditions.

Each case admits a similarity solution. These will be presented in the following section.

2.3 Similarity solutions

The models presented in Sections 2.1 and 2.2 admit similarity solutions with respect to the similarity variable

$$\eta = \frac{z}{\sqrt{4\kappa t}}.$$

Each interface can be described by

$$h(t) = 2\lambda\sqrt{\kappa t},$$

for which λ is a fixed value, in terms of the similarity variable, describing the interface. The similarity solutions presented here include assumptions of uniform thermal properties and negligible latent, but more general similarity solutions can be found in Worster (1986) and Anderson (2003). The error function and the complementary error function, which arise frequently throughout the remainder of this chapter, are defined as

$$\text{erf}(x) = \frac{2}{\sqrt{\pi}} \int_0^x \exp(-z^2)\, dz,$$

$$\text{erfc}(x) = 1 - \text{erf}(x).$$

In the case of the Stefan problem in Section 2.1, we find that

$$T(\eta) = T_B + (T_\infty - T_B)\text{erf}(\eta), \tag{2.17a}$$

$$C(\eta) = \begin{cases} C_0 + \dfrac{(C_h - C_0)\text{erfc}\left(\eta/\sqrt{\epsilon}\right)}{\text{erfc}\left(\lambda_S/\sqrt{\epsilon}\right)} & \lambda_S < \eta, \\ 0, & 0 < \eta < \lambda_S, \end{cases} \tag{2.17b}$$

where

$$C_h = -\left(T_B - T_M + (T_\infty - T_B)\text{erf}(\lambda_S)\right)/\Gamma, \tag{2.17c}$$

and λ_S, which describes the solid-liquid interface position, is the root of

$$2\lambda C_h = \frac{2(C_h - C_0)}{\sqrt{\pi}\sqrt{\epsilon}\,\text{erfc}(\lambda/\sqrt{\epsilon})} \exp\left(\frac{-\lambda^2}{\epsilon}\right). \tag{2.17d}$$

In the presence of a mushy layer with a noneutectic solid-mush front, described by (2.9a)-(2.15), we find that

$$T(\eta) = T_B + (T_\infty - T_B)\text{erf}(\eta), \tag{2.18a}$$

$$C(\eta) = \begin{cases} C_0 + \dfrac{(C_h - C_0)\text{erfc}\left(\eta/\sqrt{\epsilon}\right)}{\text{erfc}\left(\lambda_b/\sqrt{\epsilon}\right)} & \lambda_b < \eta, \\ -(T(\eta) - T_M)/\Gamma, & \lambda_a < \eta < \lambda_b, \\ 0, & 0 < \eta < \lambda_a, \end{cases} \tag{2.18b}$$

where

$$C_h = -\left(T_B - T_M + (T_\infty - T_B)\text{erf}(\lambda_b)\right)/\Gamma, \tag{2.18c}$$

and λ_a and λ_b, which respectively describe the solid-mush and mush-liquid interface positions, are the roots of

$$0 = 2\lambda_a C_{a+} + \epsilon C'_{a+}, \tag{2.18d}$$

$$\exp\left(\left(\frac{1}{\epsilon} - 1\right)\lambda_b^2\right) = \frac{-\Gamma C_0 - T(\lambda_b)}{\sqrt{\epsilon}(T_\infty - T_B)\mathrm{erfc}(\lambda_b/\sqrt{\epsilon})}, \tag{2.18e}$$

where C' is the derivative of C with respect to the similarity variable η.

In the presence of a mushy layer with a eutectic solid-mush front, described by (2.9a)-(2.15) but with (2.13a)-(2.13c) replaced by (2.16a)-(2.16d),

$$T(\eta) = T_B + (T_\infty - T_B)\mathrm{erf}(\eta), \tag{2.19a}$$

$$C(\eta) = \begin{cases} C_0 + \frac{(C_h - C_0)\mathrm{erfc}\left(\eta/\sqrt{\epsilon}\right)}{\mathrm{erfc}\left(\lambda_b/\sqrt{\epsilon}\right)} & \lambda_b < \eta, \\ -(T(\eta) - T_M)/\Gamma, & \lambda_E < \eta < \lambda_b, \end{cases} \tag{2.19b}$$

$$\mathscr{C}(\eta) = \left(C_E + \frac{\epsilon C'_{a+}}{2\lambda_E}\right)\chi_{a+}, \ (0 < \eta < \lambda_E) \tag{2.19c}$$

where

$$C_h = -\left(T_B - T_M + (T_\infty - T_B)\mathrm{erf}(\lambda_b)\right)/\Gamma, \tag{2.19d}$$

and λ_b and λ_E, which describe the mush-liquid and eutectic solid-mush interface positions, are the roots of

$$\exp\left(\left(\frac{1}{\epsilon} - 1\right)\lambda_b^2\right) = \frac{-\Gamma C_0 - T(\lambda_b)}{\sqrt{\epsilon}(T_\infty - T_B)\mathrm{erfc}(\lambda_b/\sqrt{\epsilon})}, \tag{2.19e}$$

$$\mathrm{erf}(\lambda_E) = (T_E - T_B)/(T_\infty - T_B). \tag{2.19f}$$

In each of the two cases where a mushy layer is present, we also need to identify the liquid fraction throughout the mush. For $\lambda_a \leq \eta \leq \lambda_b$,

$$\chi(\eta) = \chi_b \exp\left(\int_\eta^{\lambda_b} \frac{\epsilon C''(\xi) + 2\xi C'(\xi)}{\epsilon C'(\xi) + 2\xi C(\xi)}\ d\xi\right), \tag{2.20}$$

where $\chi_b = 1$ due to the combination of our assumptions with the condition of marginal equilibrium. In more general circumstances, where thermal properties are not uniform and latent heat is present, Worster (1986) demonstrates that $\chi_b = 1$ does not always hold.

One additional fact in the case of the noneutectic solid-mush front is that $\chi_a = 0$. This is the result of the integrand in (2.20) having a singularity at $\eta = \lambda_a$, due to the condition (2.18d). Analysis of the differential equation governing the liquid fraction in the mushy layer illuminates this more clearly, and the full proof is provided in Appendix A.

2.4   Switching temperatures

A careful study of the solutions in Section 2.3 indicate that there are two possibilities for the solid-mush interface in the presence of a mushy layer whenever $T_B < T_E$. Only one of these fronts can occur for a given set of parameters, since both fronts behave like $\alpha t^{1/2}$ with different coefficients, so it is important to correctly identify which interface conditions
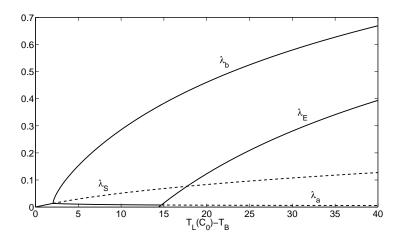
Figure 2.1: The various interface positions are shown as functions of the difference $T_L(C_0) - T_B$. The dashed curves represent the predicted positions of interfaces which are not actually present at a particular base temperature.

should be applied. At a basic level, we should expect that the front that advances at a faster rate should be the one that is present. Everything below a eutectic front must be solid, based on the phase diagram, so if the eutectic front advances more rapidly than the predicted noneutectic front then clearly the eutectic front should be present. Additionally, it is important to correctly identify whether a mushy layer will even appear.

For a given set of parameters, the solution to the Stefan problem can be computed and checked for supercooling ahead of the front. If supercooling is not present, then that was the correct solution. If supercooling is present, then the solution to the mushy layer problem with a noneutectic front can be computed, and the temperature at the solid-mush front can be compared with the eutectic temperature. If that temperature is above the eutectic, then the mushy layer solution with a noneutectic solid-mush front is correct. Otherwise, the mushy layer solution with a eutectic solid-mush front is the correct solution.

For a given alloy with a specific concentration, it would be convenient to know the values of T_∞ and T_B where each of the three models applies. If we fix one of these two values, say T_∞, then we can identify two critical values of T_B at which the system transitions from a solid-liquid interface to having a mushy layer with a diffusion-controlled solid-mush interface and then to a eutectic solid-mush interface.

In figure 2.1 we demonstrate the predicted positions of the interface positions λ_i, in terms of the similarity variable, with respect to the difference between $T_L(C_0)$ and T_B. For T_B near $T_L(C_0)$, only a liquid-solid interface appears. Once T_B is sufficiently cold for undercooling to occur at a solid-liquid interface, two interfaces bounding a mushy layer appear instead. For $T_B < T_E$, the eutectic solid-mush interface can be predicted, but the noneutectic interface dominates for a relatively narrow range of T_B values. However, once T_B crosses some critical value T_B^*, the eutectic solid-mush front begins to dominate the noneutectic solid-mush front.

2.4.1 Transition from Stefan problem to mushy layer problem

For the Stefan problem with our assumptions, supercooling ahead of the interface leads to instability of the front. This instability leads to the presence of a mushy layer, so the condition that becomes important for the transition is

$$\left(\frac{\partial T}{\partial z}\right)_{h^+} = -\Gamma \left(\frac{\partial C}{\partial z}\right)_{h^+}. \tag{2.21}$$

If this condition is satisfied at the critical value of T_B, which we will denote $T_B^\dagger$, then we can use the similarity solution given by (2.17a)-(2.17d) to rewrite the condition as

$$2(T_\infty - T_B^\dagger) \exp\left(-\lambda_S^2\right) + \left(\frac{\Gamma C_0 - T_M + T_B^\dagger + \left(T_\infty - T_B^\dagger\right)\operatorname{erf}(\lambda_S)}{\operatorname{erfc}(\lambda_S/\sqrt{\epsilon})}\right) \exp\left(\frac{-\lambda_S^2}{\epsilon}\right) = 0, \tag{2.22}$$

where λ_S is a function of T_B, determined by (2.17d).

2.4.2 Transition between solid-mush interface types

The transition between the two different solid-mush interface types can be described as when the two coincide. We will denote the critical value of T_B where this occurs as T_B^*. The diffusion-controlled interface satisfies (2.13a)-(2.13c) and the eutectic interface satisfies (2.16a)-(2.16d). In terms of the similarity solutions, the diffusion-controlled interface satisfies

$$\chi_{a^+} = 0, \tag{2.23a}$$

$$C_{a^+} + \frac{\epsilon}{2\lambda_a}C'_{a^+} = 0, \tag{2.23b}$$

and the eutectic interface satisfies

$$\left(C_E + \frac{\epsilon}{2\lambda_a}C'_{a^+}\right)\chi_{a^+} = \mathscr{C}_{a^-}, \tag{2.24}$$

when $\lambda_a = \lambda_E$ and $T_B = T_B^*$. Furthermore, when $\lambda_a = \lambda_E$, we see that $\mathscr{C}_{a^-} = 0$, so

$$C_E + \frac{\epsilon}{2\lambda_a}C'_{a^+} = 0, \tag{2.25a}$$

with

$$\operatorname{erf}(\lambda_a) = \frac{T_E - T_B^*}{T_\infty - T_B^*}. \tag{2.25b}$$

We can manipulate (2.25a) using the liquidus relationship (2.12c) to get the condition

$$2\lambda_a \left(T_E - T_M\right) + \epsilon T'_{a^+} = 0, \tag{2.26}$$

where λ_a is the solution to (2.25b).

2.4.3 Regimes

Combining the results of the previous parts of this section, we can numerically identify the two values $T_B^\dagger$ and T_B^*. We can use such results with varying T_∞ to identify regions where each of the models applies. Such results are summarized in figure 2.2. In that figure, a portion of the $T_\infty - T_B$ plane is separated into three distinct regions, one where there is no mushy layer, one where the diffusion-controlled solid-mush front appears, and one where the eutectic solid-mush front is present. As with other calculations in this dissertation, we have utilized the parameters in Set 1 of Table 1 from Worster (1986), roughly approximating a 14% $NaNO_3 + H_2O$ solution, for which we have assumed that $C_E = 0.5$ for convenience.
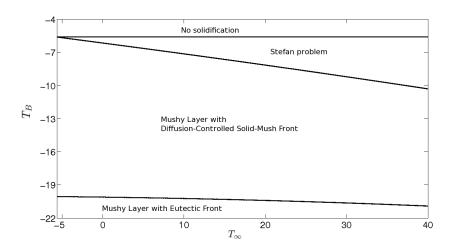
Figure 2.2: The horizontal line at $T_B = T_L(C_0) = -5.6$ is the temperature needed to initiate solidification. The middle curve describes the critical temperature $T_B^\dagger$ at the bottom of the tank at which a mushy layer first appears. The lower curve describes the critical temperature T_B^* at the bottom of the tank at which the solid-mush front transitions to a eutectic front. In other words, the curves divide the $T_E - T_B$ plane into four regions: the top region where no solidification occurs, the upper middle region where a solid-liquid front appears, the lower middle region where a mushy layer appears with a noneutectic solid-mush front, and the lower region where a mushy layer appears with a eutectic solid-mush front.

Chapter 3

Finite domain case without eutectic effects

The assumption of an infinite domain, as exhibited in the previous chapter, can lead to a mushy layer that grows forever. In the experimental arrangement where a tank filled with a uniformly mixed solution is placed upon a cold boundary, with fixed temperature at the upper boundary, the growth of the mushy layer is restricted by the thermal profile within the tank. As will be demonstrated, if the diffusion of solute is ignored, then a mushy layer can be present for all time, whereas the presence of solute diffusion will result in the eventual elimination of the mushy layer. In this chapter, we focus on the finite domain mushy layer model without the presence of eutectic effects. Much of the work presented in this chapter appears in Gewecke and Schulze (2011).

3.1 Mushy layer problem on a finite domain

The model on a finite domain is similar to the model presented for an infinite domain. The farfield conditions are replaced by conditions at an upper boundary $z = H$, specifically

$$T(H, t) = T_H, \tag{3.1a}$$

$$\frac{\partial C}{\partial z}(H, t) = 0, \tag{3.1b}$$

where $T_H > T_L(C_0)$. The first condition represents a fixed temperature at the upper boundary. The second condition represents no flux of solute at the upper boundary, which is necessary for conservation of solute. In addition to this modification, the liquid region becomes the region $b(t) < z < H$. The temperature at the bottom of the tank is chosen in the range $T_E \leq T_B < T_L(C_0)$.

We will nondimensionalize the system in order to highlight the controlling parameters of the system. We rescale the temperature, time, and space variables using

$$\theta = \frac{T - T_B}{T_H - T_B}, \qquad \hat{t} = \frac{\kappa}{H^2} t, \qquad \hat{z} = \frac{1}{H} z.$$

The concentration and liquid fraction already vary between zero and one; they are scaled naturally to be fractional values without units. We will drop the 'hats' on the variables, so

the variables throughout the rest of this chapter refer to these rescaled quantities, unless specifically noted. We will maintain our assumption of negligible latent heat, and any nondimensional parameters will be identified when they are presented.

At the upper boundary, which is now located at $z = 1$,

$$\theta = 1, \tag{3.2a}$$

$$\frac{\partial C}{\partial z} = 0. \tag{3.2b}$$

In the liquid region, $b(t) < z < 1$,

$$\frac{\partial \theta}{\partial t} = \frac{\partial^2 \theta}{\partial z^2}, \tag{3.3a}$$

$$\frac{\partial C}{\partial t} = \epsilon \frac{\partial^2 C}{\partial z^2}, \tag{3.3b}$$

where $\epsilon = D/\kappa$ is the inverse Lewis number.

At the mush-liquid interface, $z = b(t)$,

$$[\theta]_-^+ = 0, \tag{3.4a}$$

$$\left[\frac{\partial \theta}{\partial z} \right]_-^+ = 0, \tag{3.4b}$$

$$[C]_-^+ = 0, \tag{3.4c}$$

$$\epsilon \left[\chi \frac{\partial C}{\partial z} \right]_-^+ = -C_b \left(1 - (\chi_{b-}) \right) \dot{b}. \tag{3.4d}$$

There is one remaining condition at this interface, which will be discussed in more detail in Section 3.2. The condition of marginal equilibrium, which reflects the physical idea that the mushy layer grows to relieve undercooling, will be applied only when it is needed. Due to the nature of the equations within the mushy layer, which will be presented below and discussed more thoroughly in Section 3.2, the condition of marginal equilibrium will not apply for all time. This condition can be written as

$$\left(\frac{\partial \theta}{\partial z} \right)_{b^+} = -\hat{\Gamma} \left(\frac{\partial C}{\partial z} \right)_{b^+}, \tag{3.5a}$$

when

$$\dot{b}(t) > -\epsilon \left(\frac{\partial C}{\partial z} (b^-(t), t) \right) / C(b^-(t), t), \tag{3.5b}$$

where $\hat{\Gamma} = \Gamma / (T_H - T_B)$. The condition given above indicates that the condition of marginal equilibrium holds when the interface is advancing more rapidly than the leading characteristic. When combined with the other interface conditions and our assumptions, the condition of marginal equilibrium forces

$$\chi_{b-} = 1. \tag{3.6}$$

In a more general setting with nonuniform thermal properties, the resulting value of χ_{b-} may be less than one, as indicated in Worster (1986). When the interface velocity falls below the given threshold, the value of χ_{b-} will be dictated by the evolution equation for

the liquid fraction in the mushy layer.

In the mushy layer, $a(t) < z < b(t)$,

$$\frac{\partial \theta}{\partial t} = \frac{\partial^2 \theta}{\partial z^2}, \tag{3.7a}$$

$$\frac{\partial (\chi C)}{\partial t} = \epsilon \frac{\partial}{\partial z} \left(\chi \frac{\partial C}{\partial z} \right), \tag{3.7b}$$

$$\theta = -\hat{\Gamma} \left(C - C_B \right), \tag{3.7c}$$

where $C_B = (T_M - T_B)/\Gamma$ is the liquidus concentration corresponding to T_B. In (3.7b), the diffusive flux is $\chi \frac{\partial C}{\partial z}$ instead of $\frac{\partial (\chi C)}{\partial z}$, because the diffusion occurs only within the interstitial liquid. If the concentration within this interstitial fluid were uniform but the liquid fraction were variable, we would expect no solute diffusion to occur, which indicates that our choice of the diffusive flux is correct.

At the solid-mush interface, $z = a(t)$,

$$[\theta]_-^+ = 0, \tag{3.8a}$$

$$\left[\frac{\partial \theta}{\partial z} \right]_-^+ = 0, \tag{3.8b}$$

$$C_{a^+} \chi_{a^+} \dot{a} = -\epsilon \chi_{a^+} \left(\frac{\partial C}{\partial z} \right)_{a^+}. \tag{3.8c}$$

In the solid region, $0 < z < a(t)$,

$$\frac{\partial \theta}{\partial t} = \frac{\partial^2 \theta}{\partial z^2}. \tag{3.9}$$

Since we have assumed that the solid is pure and that there is no diffusion of solute within the solid, we do not need any equations for the evolution of the concentration in the solid.

At the bottom of the tank, $z = 0$,

$$\theta = 0. \tag{3.10}$$

At $t = 0$, only liquid is present, and

$$\theta(z, 0) = 1, \tag{3.11a}$$

$$C(z, 0) = C_0. \tag{3.11b}$$

Due to continuity of θ and θ_z at the two interfaces, and since θ is governed by the diffusion equation in each of the three regions, we find that θ solves the diffusion equation on the whole domain $0 < z < 1$, subject to $\theta(0, t) = 0$ and $\theta(1, t) = 1$. This is one of the key benefits of the assumption of negligible latent heat.

3.2 Method of characteristics

We will now turn our attention to (3.7b), which holds in the mushy layer, and rewrite it as

$$\frac{\partial \chi}{\partial t} - \frac{\epsilon}{C} \left(\frac{\partial C}{\partial z} \right) \left(\frac{\partial \chi}{\partial z} \right) + \frac{1}{C} \left[\left(\frac{\partial C}{\partial t} \right) - \epsilon \left(\frac{\partial^2 C}{\partial z^2} \right) \right] \chi = 0. \tag{3.12}$$

23

Due to the liquidus relationship (3.7c), and since θ does not depend on any other quantities in this problem, this equation is a first-order partial differential equation describing the evolution of the liquid fraction. As a result, the method of characteristics can be applied to solve this equation. Applying this method, as can be found in Evans (1998) and numerous other sources, we find that the characteristics satisfy

$$\dot{\tau}(s) = 1, \tag{3.13a}$$

$$\dot{\zeta}(s) = \left(\frac{-\epsilon}{C(\zeta(s), \tau(s))} \right) \frac{\partial C}{\partial z}(\zeta(s), \tau(s)), \tag{3.13b}$$

$$\dot{\chi}(s) = \frac{1}{C(\zeta(s), \tau(s))} \left(\epsilon \frac{\partial^2 C}{\partial z^2}(\zeta(s), \tau(s)) - \frac{\partial C}{\partial t}(\zeta(s), \tau(s)) \right) \chi(s), \tag{3.13c}$$

where τ and ζ correspond to time and spatial position. Equation (3.13a) indicates that τ and t correspond directly with each other. Additionally, (3.13c) can be integrated with respect to s, so

$$\chi(s) = \chi(0) \exp \left(\int_0^s \frac{\epsilon \frac{\partial^2 C}{\partial z^2}(\zeta(\xi), \tau(\xi)) - \frac{\partial C}{\partial t}(\zeta(\xi), \tau(\xi))}{C(\zeta(\xi), \tau(\xi))} \, d\xi \right). \tag{3.14}$$

Based on the behavior of the diffusion equation, $\theta_z > 0$ on the whole domain for $t > 0$. Combining this with the liquidus relationship, we see that $C_z < 0$ throughout the mushy layer. Since $C > 0$ in the mushy layer, characteristic curves always advance, as these inequalities applied to (3.13b) yield $\dot{\zeta}(s) > 0$.

Taking into account these characteristic curves, we can address the final mush-liquid interface condition, as given by (3.5a)-(3.5b). In Worster (1986), the condition of marginal equilibrium was always enforced at the mush-liquid interface. In the special case of uniform thermal properties, this implies $\chi_b = 1$. Such a condition was appropriate because the interface in the semi-infinite domain case always advances at a sufficiently high rate, proportional to $t^{-1/2}$. In the present case, this interface cannot advance beyond the isotherm corresponding to $\theta_L(C_0)$, so the interface cannot advance at such a high rate for all time.

Examination of the characteristics can further illuminate this situation. As illustrated in figure 3.1(a), characteristic curves for the infinite-domain problem emerge from the mush-liquid front and never again intersect with the front. Thus, the advance of each characteristic is bounded below, so every characteristic curve will intersect with the mush-liquid interface in finite time. The condition $\chi_{b-} = 1$ is inconsistent with the value of χ along characteristic curves that are intersecting with the mush-liquid interface. In figure 3.1(b), we see how characteristics for the finite-domain problem intersect with the mush-liquid interface. In the case of a finite domain, the maximum height of the mush-liquid interface is restricted. Once the thermal profile reaches its linear steady state, the concentration in the mush satisfies $C_z = -1/\hat{\Gamma}$ and $0 < C \le C_E$, so

$$\dot{\zeta}(s) = \frac{-\epsilon \frac{\partial C}{\partial z}(\zeta(s), \tau(s))}{C(\zeta(s), \tau(s))} \ge \frac{\epsilon}{\hat{\Gamma} C_E}.$$

In terms of the characteristic curves, we set $\chi_{b-} = 1$, due to the condition of marginal equilibrium, whenever characteristic curves emerge from the mush-liquid interface, which occurs when the interface velocity is greater than the velocity of the leading characteristic.
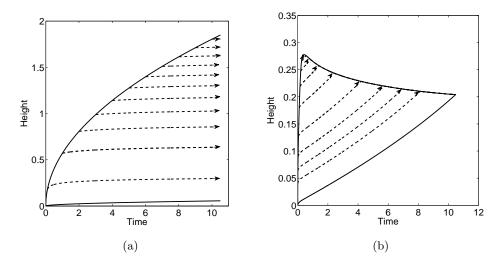
Figure 3.1: In both images, the characteristics are given by dashed curves. The solid curves denote the solid-mush interface (lower curve) and the mush-liquid interface (upper curve). The infinite domain case is shown in (a) and the finite domain case is shown in (b).

Otherwise, the value of χ_{b^-} is dictated by the liquid fraction value along the characteristic curve which intersects the interface at time t. In other words, the condition of marginal equilibrium is a physical principle which serves as a closure condition when such a condition is required. This leads to the final condition at the liquid-mush interface, given by (3.5a)-(3.5b).

An important result associated with the method of characteristics is that the solid-mush interface follows a characteristic curve. As demonstrated in the appendix, $\chi_a = 0$ for the similarity solution with no latent heat, under the assumption that eutectic effects are not present. Clearly, $\chi_{a^+} = 0$ is a solution for the free-boundary condition given by (3.8c). If $\chi(s_1) = 0$ on a particular characteristic for some value $s = s_1$, then $\chi(s) = 0$ along that entire characteristic curve, due to (3.13c). Therefore, such a characteristic would satisfy the interface condition. However, if the interface advanced more rapidly than this characteristic, then the liquid fraction at the solid-mush interface would be determined by the value along a characteristic terminating along the interface, which would result in $\chi_{a^+} \neq 0$, so (3.8c) could be rewritten as

$$\dot{a} = \frac{-\epsilon}{C_{a^+}} \left(\frac{\partial C}{\partial z} \right)_{a^+}, \tag{3.15}$$

which is (3.13b) applied at $(\zeta(s), \tau(s)) = (a(t), t)$. This indicates that the advance of the interface is the same as the advance of a characteristic, which contradicts the assumption that the interface advanced more rapidly than a characteristic. Therefore, the solid-mush interface travels along a characteristic with $\chi_{a^+} = 0$. Furthermore, since all characteristics intersect the mush-liquid interface in finite time, the solid-mush interface will do the same. As a result, the mushy layer will completely disappear in finite time.

3.3 Steady states

An important difference between the cases where solute diffusion is present and where it is absent appears in the associated steady states. In the case $\epsilon = 0$, where solute diffusion is assumed to be negligible, the steady state is given by

$$\theta(z) = z,$$
$$C(z) = \begin{cases} C_0, & \hat{\Gamma}(C_B - C_0) \le z \le 1, \\ \frac{\hat{\Gamma}C_B - z}{\hat{\Gamma}}, & 0 \le z \le \hat{\Gamma}(C_B - C_0) \end{cases}$$
$$\chi(z) = \begin{cases} 1, & \hat{\Gamma}(C_B - C_0) \le z \le 1, \\ \frac{\hat{\Gamma}C_0}{\hat{\Gamma}C_B - z}, & 0 \le z \le \hat{\Gamma}(C_B - C_0). \end{cases} \tag{3.16}$$

Note that this steady state does not include a solid region.

In the case $\epsilon > 0$, where solute diffusion is present, the steady state is given by

$$\theta(z) = z,$$
$$C(z) = \begin{cases} 0, & 0 \le z < h^* \\ \frac{C_0}{1 - h^*}, & h^* \le z \le 1, \end{cases} \tag{3.17}$$
$$\chi(z) = \begin{cases} 0, & 0 \le z < h^* \\ 1, & h^* \le z \le 1, \end{cases}$$
$$h^* = \frac{1}{2}\left(1 + \hat{\Gamma}C_B - \sqrt{\left(1 - \hat{\Gamma}C_B\right)^2 + 4\hat{\Gamma}C_0}\right). \tag{3.18}$$

Note that this steady state does not include a mushy region. Instead, there is a solid region in equilibrium with a liquid region of increased concentration.

From the above, we see that the assumption of negligible solute diffusion results in a steady-state mushy zone, but the presence of diffusion eliminates that mushy zone and results in a phase-separated steady state.

3.4 Numerical method

The full model with nonzero latent heat poses many challenges numerically. At each time step, the positions of the two free interfaces must be determined. The coupled partial differential equations in the mush require careful consideration. In addition, calculations of the solutions of the differential equations in each of the three regions depends upon the interface locations, which themselves depend upon the solutions of the differential equations. Accurately solving for the liquid fraction requires the solution of a first-order partial differential equation, which requires upwinding to be performed in the correct direction.

The assumption of negligible latent heat alleviates a number of these challenges. The key benefit is that the temperature field no longer depends upon the liquid fraction in the mush, but is instead governed by the heat equation over the whole domain. This allows the temperature field to be calculated separately from all other quantities in the problem. Applying the method of characteristics allows us to track the liquid fraction using a simple formula, and it allows us to track the solid-mush interface position without any additional effort since this interface follows a characteristic. Once the temperature field has been

calculated, we utilize the liquidus relationship to determine the concentration values in the mush. This leaves two quantities whose numerical solutions rely heavily on each other: concentration in the liquid region and the mush-liquid interface position.

While the numerical procedure utilized here will not directly translate to the nonzero latent heat case, the intent is to generate a relatively simple procedure to gain insight into various behaviors of the system. These insights can then inform future construction of a numerical procedure which will include the latent heat terms. We first present the various spatial discretizations used and proceed with a description of the numerical scheme.

3.4.1 Discretization

The discretizations of the various quantities in this problem are handled in different ways. Essentially, the simplest discretizations that worked well were utilized.

For liquid fraction within the mush, we do not utilize a spatially uniform discretization. Instead, we track the characteristics within the mush. The temperature field is tracked independently of the characteristics, which allows for this choice.

A spatially uniform mesh over the entire domain is utilized for the temperature field. The interface positions do not influence the temperature field at all, so splitting the domain for the temperature field into three pieces would introduce unnecessary complications. Since we use characteristics to track the liquid fraction in the mush, additional work is required to incorporate data for the concentration in the mush to solve the characteristic equations, where the concentration in the mush is determined by the liquidus relationship. Either a non-uniform mesh or interpolation is required. We utilize interpolation since interpolating the data seems the better approach and solving for the temperature field on the whole domain is easier than solving on three domains.

The concentration only needs to be solved for in the liquid region. For this, we use a spatially uniform mesh. This domain is dependent upon time, so the mesh varies with time. To handle this, we map the liquid region $[b(t), 1]$ to the fixed domain $[0, 1]$. Specifically, the transformation is given by

$$\tau = t, \ \xi = \frac{z - b(t)}{1 - b(t)}.$$

This transformation changes (3.3b) into

$$\frac{\partial C}{\partial \tau} - \frac{(1 - \xi)\dot{b}(\tau)}{H - b(\tau)} \frac{\partial C}{\partial \xi} = \frac{\epsilon}{(H - b(\tau))^2} \frac{\partial^2 C}{\partial \xi^2}. \tag{3.19}$$

The gridpoints in $[0, 1]$ do not move, so data at the previous timestep can be utilized directly. This transformation introduces a first-order spatial derivative which accounts for the movement of the gridpoints in the original variables.

3.4.2 Scheme

We initialize the system at some very small initial time t_s using the similarity solution from Worster (1986) discussed in Section 2.3. A small number of characteristics are initiated at this time, including a characteristic at each of the two interfaces. In line with the fact that the liquid fraction along the solid-mush interface is zero, see Appendix A, the corresponding characteristic is initiated with $\chi = 0$.

For each following timestep t_i, we perform the following steps:

1. We update the temperature distribution over the whole domain, using the implicit Euler scheme.

2. For each characteristic present at t_{i-1}, we update the position and liquid fraction data, assuming that all characteristics remain in the mush. The values for concentration and its derivatives are calculated using the liquidus relationship and interpolating the values of θ and its derivatives. The new position for each characteristic is identified through the trapezoid rule for ordinary differential equations and a Newton iteration. The liquid fraction is then updated using a trapezoid rule quadrature to integrate from t_{i-1} to t_i, as (3.14) can be rewritten to get

$$\chi(t_i) = \chi(t_{i-1}) \exp\left(\int_{t_{i-1}}^{t_i} \frac{\epsilon \frac{\partial^2 C}{\partial z^2}(\zeta(\xi), \tau(\xi)) - \frac{\partial C}{\partial t}(\zeta(\xi), \tau(\xi))}{C(\zeta(\xi), \tau(\xi))} \, d\xi\right).$$

Since the solid-mush interface follows a characteristic, this procedure also updates the interface position a_i.

3. We then determine the location of the mush-liquid interface b_i:

   (i) We guess an interface position b_i and a secondary guess $b_i + \delta$, with δ small.

   (ii) The concentration field in the liquid is calculated using the two guess values above.

   (iii) For each guess, the liquid fraction at the mush-liquid interface is set to unity if the guess is ahead of the leading characteristic or to an interpolated value if the guess is behind the leading characteristic. Specifically, we determine the two characteristics bounding the guess, then interpolate the liquid fraction values between those characteristics. Residuals for each of the two guesses are then calculated using (3.4d).

   (iv) Using the residuals calculated in the previous step, we use a secant-line approximation of the derivative in a Newton iteration to update the guess for b_i. With this updated guess, we repeat the previous two steps.

   (v) Once the size in the change for the guess is small enough, we terminate the iteration. If the accepted value of b_i is ahead of the leading characteristic, we initialize a characteristic at (b_i, t_i) with $\chi = 1$. If the accepted value of b_i is not ahead of the leading characteristic, we remove characteristics as needed so that the leading characteristic is at (t_i, b_i). In practice, we remove characteristics by setting their positions at t_i to be b_i and by setting their liquid fraction values to the value determined for the interface position. We then proceed to the next timestep.

3.5   Results

In order to connect with potential future experiments, we will be presenting many of our results in terms of the unscaled variables. All graphs will be in terms of the scaled variables. The parameters used to generate our results, as given in Table 1.1, roughly approximate a 14% sodium nitrate solution. The initial temperature of the tank T_H is taken to be 15 degrees Celsius, and the temperature of the cold surface T_B is taken to be -15.6 degrees

Celsius. Additionally, the tank has a height of 15 cm. These parameters correspond to the nondimensional values $\epsilon \approx 7.7 \times 10^{-3}$, $\hat{\Gamma} \approx 1.307$, $C_B = 0.39$, and the melting temperature of the pure material $T_M = 0$ corresponds to $\theta \approx 0.51$.

The interface positions through time are shown in figure 3.2. For the parameters used, the time for the mush-liquid interface to reach its maximum height of approximately 4 centimeters is approximately one day. In that time, the solid-mush interface has only reached a height of approximately 0.25 centimeters. The mush-liquid interface then begins to retreat slowly and the solid-mush interface continues a steady advance. After approximately 22 days the mush vanishes. During the retreat of the mush-liquid interface, the liquid fraction at the interface decreases. After the mush vanishes, the solid-liquid interface is shown; see Worster (1986) for the appropriate interface conditions.

In figure 3.3, we can see how the liquid fraction varies as time progresses. As long as a particular spatial point stays in the mush, the liquid fraction at that point decreases with time. In figure 3.4, we can see how the temperature profile changes. This should be recognized as the solution of the heat equation on a finite domain. In figure 3.5, we can see how the concentration profile varies in the liquid. The final concentration curve shown relates to the time when the mush vanishes.

In figure 3.6 the solution during the early times is compared with the similarity solution from Worster (1986). The curves match up very well for a significant portion of the time until the mush-liquid interface reaches its maximum height. The curve for the mush-liquid interface in the similarity solution eventually outpaces the finite-domain solution, but this is expected due to the similarity solution having no bound on how far it could advance. The solid-mush interface is well-approximated by the similarity solution over the interval shown, but it too will eventually stop advancing in the finite tank.

In figure 3.7 the solution for the mush-liquid interface during the early times is compared with the solution for $\epsilon = 0$ on a finite domain. The curves match up fairly well during the times shown. The advance of the mush-liquid interface position is well-approximated by the $\epsilon = 0$ solution, but the $\epsilon = 0$ solution does not capture the retreat of the interface, as highlighted in figure 3.8. Additionally, the $\epsilon = 0$ solution does not exhibit an advancing solid-mush interface. The absence of the solid-mush front when $\epsilon = 0$ is caused by (3.7b) transforming into

$$\frac{\partial}{\partial t}\left(\chi C\right) = 0,$$

which prevents $\chi_a = 0$, so the only permissible solution of (3.8c) is $\dot{a} = 0$.

Other trials confirm that the time scales with H^2 and the heights of the fronts scale with H, as can be predicted from the scaling of the system.

A boundary-layer analysis can also provide useful insights into the system. Consider expansions of the form

$$f(z,t) = f_0(z,t) + \epsilon f_1(z,t) + \epsilon^2 f_2(z,t) + \cdots$$

for the temperature, concentration, and liquid fraction. To leading order, the equations governing the temperature distribution do not change, but the equations governing concentration and liquid fraction change to the equations for $\epsilon = 0$. This forms the boundary layer, which corresponds to the time-frame of the rapid advance of the mush-liquid front, and has (3.16) as its steady state.

For a rescaling to large time, specifically $t \rightarrow \epsilon^{-1}t$, most of the equations change.

29
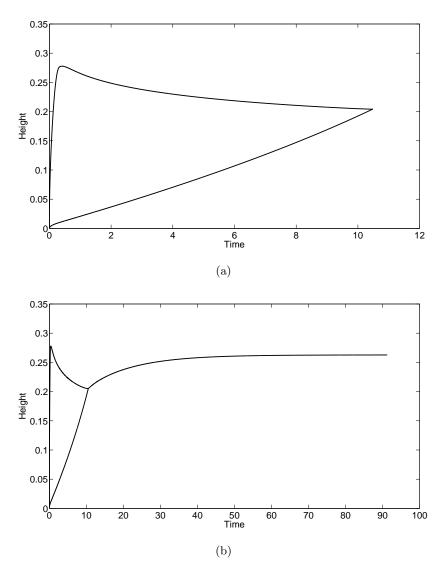
Figure 3.2: In (a), the solid-mush (lower curve) and mush-liquid (upper curve) interface positions are shown from $t = 0$ to the time when the mush vanishes. The long-time behavior is shown in (b), with only a single curve denoting the solid-liquid interface once the mush has vanished. The parameters used are provided in the main text.

(a)   (b)
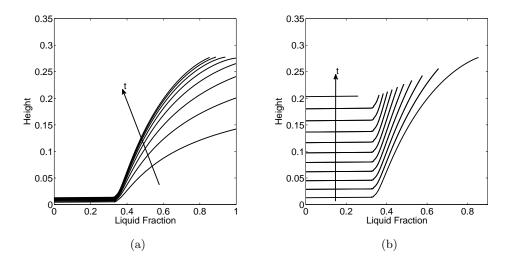
Figure 3.3: The curves are liquid fraction (χ) profiles within the mush at various stages of system evolution. The curves in (a) are at evenly-spaced intervals during the advance of the mush-liquid interface. The remainder of the time until the mush vanishes is illustrated in (b), again at evenly spaced intervals.
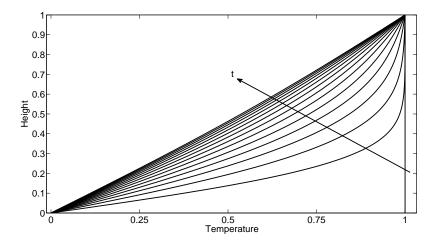
Figure 3.4: The curves shown are temperature profiles at regular intervals over the timescale for thermal diffusivity. Time progresses in the direction shown by the arrow. By the last time shown, the temperature profile is near its steady state.
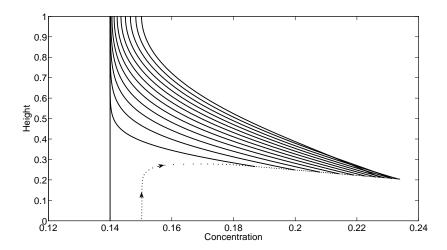
Figure 3.5: The curves shown are concentration profiles in the liquid at various stages of system evolution. The profiles shown are at evenly-spaced intervals, starting at $t = 0$. The dotted curve indicates the concentration at the mush-liquid interface. The arrows along the dotted curve indicates the direction of time progression.
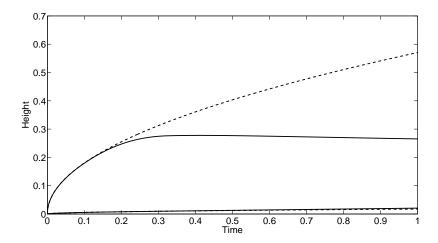
Figure 3.6: The interface positions for the finite-domain solution (solid curves) are compared with those for the infinite-domain similarity solution (dashed curves). The upper curves are the mush-liquid interfaces, and the lower curves are the solid-mush interfaces.
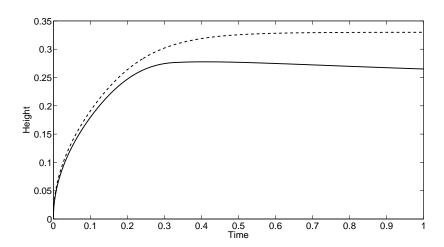
Figure 3.7: The mush-liquid interface position (solid curve) is compared with the same interface for the $\epsilon = 0$ solution (dashed curve).
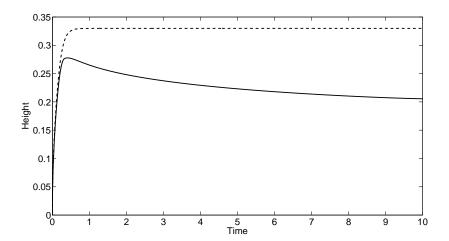
Figure 3.8: The mush-liquid interface (solid curve) for large times is compared with the corresponding interface in the $\epsilon = 0$ solution (dashed curve).

Specifically, the temperature profile becomes fixed, as the continuity of temperature and its gradients continues to hold at each interface, but in each of the three regions,

$$\frac{\partial^2 \theta}{\partial z^2} = 0.$$

Thus, the long-time solution has $\theta = z$. The concentration and liquid fraction equations transform to the equations in the system with $\epsilon = 1$. This long-time solution has (3.17) as its steady state.

Combining the above, the leading order solution for early times is the $\epsilon = 0$ solution. For large time values, the temperature solution becomes fixed, and the retreat of the mush-liquid interface and the advance of the solid-mush interface come into effect.

3.6   Remarks

Our decision to initialize the numerical scheme at some small time value is due to singularities at $t = 0$ and $z = 0$. Since $\theta(z, 0) = 1$, and then $\theta(0, t) = 0$ for $t > 0$, it is clear that θ has a discontinuity at $z = 0$, $t = 0$. By the nature of the heat equation, θ is smooth for $t > 0$. If we initialize the scheme at $t = 0$, then there is not a clear method for identifying both the location of the solid-mush interface and the liquid fraction at that interface at the next timestep. The method of characteristics is not applicable at $t = 0$ as no mush is present. To get around this issue, two options for a short-time approximation presented themselves. First, we could use the similarity solution. This option, which we chose to use, satisfies the system except at the upper boundary. However, for short times, the error presented at the upper boundary is quite small. The error for the temperature is small due to the rapid convergence of the error function to unity, and the error for the concentration gradient is small due to the rapid decay of $\exp(-\eta^2/\sqrt{\epsilon})$. For the initial time values utilized in our calculations, this error appeared to be within machine accuracy. The second option would be to use the leading order short-time solution, as appears in our boundary layer discussion. The advantage is that this approximation satisfies the boundary conditions. However, the drawbacks to such an approximation are that it only satisfies the governing equations and interface conditions to leading order and no solid layer appears at the initial time.

Code runs performed to compare the two options indicate no great disparity. After initial transients, the two are strikingly similar. The most notable differences are at the solid-mush interface, as the leading-order approximation has no solid region. This leads to the solid-mush interface lagging behind the position predicted with the similarity solution initialization, and so the mushy layer persists for a slightly longer duration. Additionally, the liquid fraction at the solid-mush interface is nonzero for the leading-order approximation. Transient effects at early time steps persist along the characteristic curves, and the differences in these effects are also perceptible.

Le Bars and Worster (2006) developed a numerical scheme for an enthalpy formulation of the mushy layer problem on a finite domain. One of the test cases in that study was simulating the semi-infinite domain similarity solution from Worster (1986), and good agreement was found until the effects of the finite domain were felt. Specifically, the growth rates of the two interfaces calculated by the numerical scheme were compared with those predicted for the similarity solution, with good agreement. These results reinforce our assertion that the similarity solution is a reasonable short-time approximation for the finite-domain problem.

Chapter 4

Finite domain case with eutectic effects

In this chapter, we will remove the restriction $T_B \geq T_E$, so that eutectic effects can be present. In the infinite domain case, as discussed in Chapter 2, two different sets of conditions are possible at the solid-mush interface, specifically a diffusion-controlled interface and a eutectic front. The correct set of conditions to apply is dictated by the specific parameters in the problem. For a given mixture and initial temperature, the interface type that appears relies entirely upon the temperature T_B at the lower boundary. Since the similarity solution provides insight into the early time behavior of the finite domain case, the temperature T_B at the lower boundary indicates which interface type initially appears.

Isotherms in the finite domain case initially advance rapidly, but they slow as the thermal profile approaches its linear steady state. As a result, we know that the isotherm associated with the eutectic temperature T_E will stop at a finite height. As we saw in Section 3.2, characteristics will always advance, including a characteristic representing the diffusion-controlled interface position. From this, we expect that if a eutectic front appears at early times, it will give way to a diffusion-controlled interface as the thermal profile approaches its steady state.

4.1   Model

The model here is similar to the model given in Chapter 3. However, we will use a modified scaling of the variables, namely

$$\theta = \frac{T - T_E}{T_H - T_E}, \qquad \hat{t} = \frac{\kappa}{H^2} t, \qquad \hat{z} = \frac{1}{H} z.$$

The cold temperature T_B at the bottom of the tank will correspond to a temperature θ_B. If $T_B \geq T_E$, then $\theta_B \geq 0$, and the results from Chapter 3 apply. On the other hand, if $T_B < T_E$, then $\theta_B < 0$ and eutectic effects may appear.

As before, we will drop the 'hats' from the variables, and any references to the variables will refer to the nondimensional variables unless otherwise noted.

The boundary conditions at the upper boundary (now $z = 1$) are

$$\theta = 1, \tag{4.1a}$$

$$\frac{\partial C}{\partial z} = 0. \tag{4.1b}$$

In the liquid region $b(t) < z < 1$,

$$\frac{\partial \theta}{\partial t} = \frac{\partial^2 \theta}{\partial z^2}, \tag{4.2a}$$

$$\frac{\partial C}{\partial t} = \epsilon \frac{\partial^2 C}{\partial z^2}, \tag{4.2b}$$

where $\epsilon = D/\kappa$ is the inverse Lewis number.

At the mush-liquid interface $z = b(t)$,

$$[\theta]_-^+ = 0, \tag{4.3a}$$

$$[C]_-^+ = 0, \tag{4.3b}$$

$$\left[\frac{\partial \theta}{\partial z}\right]_-^+ = 0, \tag{4.3c}$$

$$C_b(1 - \chi_b)\dot{b} = \epsilon \chi_b \left(\frac{\partial C}{\partial z}\right)_{b^-} - \epsilon \left(\frac{\partial C}{\partial z}\right)_{b^+}. \tag{4.3d}$$

Recall that an additional condition applies at the mush-liquid interface, specifically

$$\chi_b = 1 \text{ when } \dot{b}(t) > \dot{\zeta}_b(t), \tag{4.3e}$$

where

$$\dot{\zeta}_b(t) = -\epsilon \left(\frac{\partial C}{\partial z}(b^+(t), t)\right) / C(b^+(t), t), \tag{4.3f}$$

describes the propogation of the leading characteristic. This condition was discussed in detail in Chapter 3.

In the mushy layer $a(t) < z < b(t)$ the equations become

$$\frac{\partial \theta}{\partial t} = \frac{\partial^2 \theta}{\partial z^2}, \tag{4.4a}$$

$$\frac{\partial (\chi C)}{\partial t} = \epsilon \frac{\partial}{\partial z} \left(\chi \frac{\partial C}{\partial z}\right), \tag{4.4b}$$

$$\theta = -\hat{\Gamma}(C - C_E), \tag{4.4c}$$

where $\hat{\Gamma} = \Gamma/(T_H - T_E)$.

At the solid-mush interface $z = a(t)$ the conditions can vary, depending upon whether the solid-mush interface is a eutectic or non-eutectic front. At this interface, $\theta \geq 0$ is

required. When it is non-eutectic, that is when $\theta(a(t), t) > 0$, the conditions become

$$[\theta]_-^+ = 0, \qquad (4.5a)$$

$$\left[\frac{\partial \theta}{\partial z}\right]_-^+ = 0, \qquad (4.5b)$$

$$C_{a^+} \chi_a \dot{a} = -\epsilon \chi_a \left(\frac{\partial C}{\partial z}\right)_{a^+}. \qquad (4.5c)$$

On the other hand, when $\theta(a(t), t) = 0$ a eutectic front is present and the conditions become

$$[\theta]_-^+ = 0, \qquad (4.6a)$$

$$\theta = 0, \qquad (4.6b)$$

$$(\mathscr{C}_{a^-} - C_{a^+} \chi_{a^+}) \dot{a} = \epsilon \chi_{a^+} \left(\frac{\partial C}{\partial z}\right)_{a^+}. \qquad (4.6c)$$

The final condition above describes the amount of solute frozen into the solid. Once again, due to the liquidus relationship within the mush, the concentration on the mush side of the interface is

$$C_{a^+} = C_E.$$

In the solid $0 < z < a(t)$, solute may be present, but it does not diffuse. Heat still diffuses, so

$$\frac{\partial \theta}{\partial t} = \frac{\partial^2 \theta}{\partial z^2}, \qquad (4.7)$$

$$\frac{\partial \mathscr{C}}{\partial t} = 0. \qquad (4.8)$$

At the bottom boundary $z = 0$,

$$\theta = \theta_B, \qquad (4.9)$$

where $\theta_B = (T_B - T_E)/(T_H - T_E)$.

4.2 Method of characteristics

The method of characteristics in this case is the same as presented in Section 3.2. Characteristics still initiate along the liquid-mush interface. However, characteristics can now terminate on the solid-mush interface as well as the liquid-mush interface. For example, figure 4.1 shows characteristics initiating on the mush-liquid interface and terminating on the eutectic solid-mush interface. This is a result of the eutectic solid-mush interface advancing more rapidly than the speed of the characteristic at the solid-mush interface, which would describe the advance of the diffusion-controlled interface. Terminating characteristics dictate the liquid fraction on the mush side of the solid-mush interface, contributing to the computation of the concentration being frozen into the solid via (4.6c).

In much the same way that conditions at the mush-liquid interface were determined based on whether the interface advanced more rapidly than the leading characteristic, we can determine which solid-mush interface is present based on a comparison of the interface velocity and the velocity of the trailing characteristic. In particular, the eutectic front is
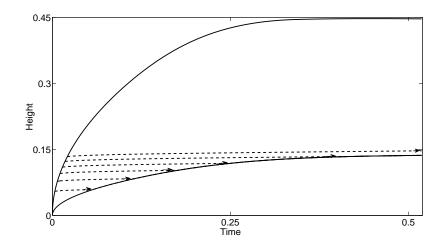
Figure 4.1: Characteristics terminate along a eutectic solid-mush interface. The solid curves are the solid-mush (lower) and mush-liquid (upper) interfaces, and the dashed curves are characteristics. The characteristics shown begin at evenly-spaced time intervals.

present if

$$\dot{a}(t) > -\epsilon \left(\frac{\partial C}{\partial z}(a^+(t), t) \right) / C(a^+(t), t), \tag{4.10}$$

and the diffusion-controlled front is present otherwise.

4.3 Numerical method

For the case with eutectic effects, we modify the method presented in Section 3.4 so that it includes the possible eutectic solid-mush interface. The previous discretizations remain the same, but now the concentration in the solid region also needs to be tracked. Previously, the solid was pure, so the concentration was zero throughout the solid and we did not need to explicitly keep track of this. Since we neglect solute diffusion in the solid, the concentration that is frozen in at time t_0 at height $a(t_0)$ remains at height $a(t_0)$ for all later time. Since we already record the solid-mush interface position as a function of time, we can simply record the concentration frozen into the solid at the interface as a function of time. The numerical scheme for this case is then the following.

   We initialize the system at some very small initial time t_s using one of the two similarity solutions. To pick between the two, we calculate the switching temperature T_B^* using the method outlined earlier and compare with our prescribed value of T_B. A small number of characteristics are initiated at this time, including a characteristic at each of the two interfaces.

   For each following timestep t_i, we do the following:

1. We update the temperature distribution over the whole domain.

2. For each characteristic present at t_{i-1}, we update the position and liquid fraction data, assuming that all characteristics remain in the mush. The values for concentration and its derivatives are calculated using the liquidus relationship and interpolating the values of θ and its derivatives.

3. We determine the location of the solid-mush interface a_i. Since the noneutectic solid-mush interface follows a characteristic, we first check to see if the corresponding characteristic has temperature above or below T_E. If it is above that temperature, then we accept that position as the interface position, set the concentration on the solid side of the interface to zero, and proceed to the next step. If the temperature is instead at or below the eutectic, we perform the following steps:

   (i) Perform a search to identify the position of the $T = T_E$ isotherm. This position will be a_i.

   (ii) The liquid fraction on the mush side of the interface is determined by the characteristics terminating on the interface.

   (iii) We calculate the concentration on the solid side of the interface, using (4.6c).

   (iv) The characteristics which terminated along the solid-mush interface, which are those whose positions had been calculated to be below the new interface position, are removed. In practice, the locations of these characteristics and the liquid fraction along these characteristics are set to the values at the interface.

4. We then determine the location of the mush-liquid interface b_i:

   (i) We guess an interface position b_i and a secondary guess $b_i + \delta$, with δ small.

   (ii) The concentration field in the liquid is calculated using the two guess values above.

   (iii) Residuals for each of the two guesses are calculated using (4.3d).

   (iv) Using the residuals calculated in the previous step, we use a secant-line approximation of the derivative in a Newton iteration to update the guess for b_i. With this updated guess, we repeat the previous two steps.

   (v) Once the size in the change for the guess is small enough, we terminate the iteration. If the accepted value of b_i is ahead of the leading characteristic, we initialize a characteristic at (b_i, t_i) with $\chi = 1$. If the accepted value of b_i is not ahead of the leading characteristic, we remove characteristics as needed so that the leading characteristic is at (t_i, b_i). In practice, the locations of such characteristics and their corresponding liquid fractions are set to the values at the interface. We then proceed to the next timestep.

4.4 Results

As in Chapter 3, the dimensional parameters used for our numerical results are provided in Table 1.1. Additionally, we set $C_E = 0.5$ and $T_E = -20$ degrees Celsius, primarily for convenience. Even though this is certainly not the true eutectic point, the qualitative behavior of the system will remain the same. We additionally set $T_H = 15$ degrees Celsius and $T_B = -25.6$ degrees Celsius, with the height of the tank being $H = 15$ cm. These parameter values correspond to the nondimensional quantities $\epsilon \approx 7.7 \times 10^{-3}$, $\hat{\Gamma} \approx 1.143$, and $\theta_B = -0.16$. For reference, the melting temperature of the pure material $T_M = 0$ corresponds to $\theta \approx 0.57$.
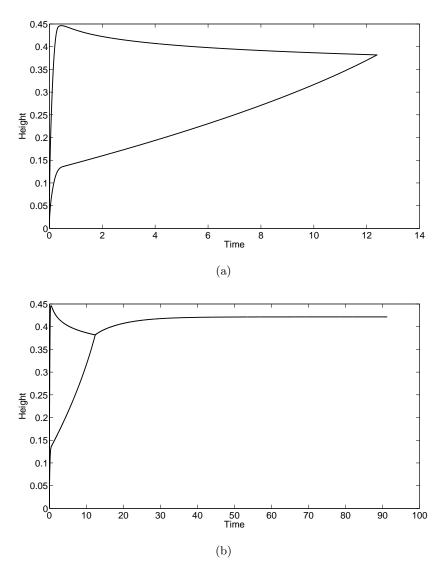
Figure 4.2: In (a), the solid-mush (lower curve) and mush-liquid (upper curve) interface positions are shown from $t = 0$ to the time when the mush vanishes. The long-time behavior is shown in (b), with only a single curve denoting the solid-liquid interface once the mush has vanished. The parameters used are provided in the main text.

In figure 4.2 we plot the interface positions are plotted in terms of the original variables, with the first image demonstrating the evolution until the mush vanishes, and the second extending out over a longer time with the solid-liquid front shown.

We demonstrate the evolution of the concentration profile in figure 4.3. We see that the solid-mush front never retreats, so the solute that is frozen into the solid at the interface remains in the same place forever. The concentration on the solid side of the interface is plotted as a function of time in figure 4.4, to highlight the fact that the amount of solute being frozen into the solid declines over time, eventually becoming negligible once the evolution of the temperature field has stagnated sufficiently. Once that occurs, the solid-mush front switches from a eutectic front to a noneutectic front. In figure 4.4(b), the vertical line represents the concentration in the solid determined by the semi-infinite domain model in Chapter 2. There is good agreement between the two models over a large portion of this region.

The evolution of the temperature profile is given in figure 4.5, and should be recognized as the solution to the heat equation on a finite domain. The evolution of the liquid fraction in the mushy zone is given in figure 4.6.

Another important aspect is how this solution compares with the solution that would be generated if we were to ignore the possibility of a $T = T_E$ front. Figure 4.7 shows the interface positions generated in the present case along with the interface positions generated by utilizing the method set forth in Section 3.4, ignoring the impact of eutectics. We see three major impacts. The most easily predicted impact is that the solid-mush interface advances much more rapidly at early times when the $T = T_E$ front is incorporated. Next, we see that the time until the mush vanishes is reduced. This is primarily due to the rapid advance of the solid-mush front at early times. Finally, we can see that the eventual steady states are different, with the solid-liquid interface advancing farther when the $T = T_E$ interface is incorporated. This is also predictable, as some of the solute becomes incorporated in the solid, so there is less total solute in the liquid in this long-time regime. Since the steady-state location of the solid-liquid interface is dictated by the liquidus relationship, with the concentration being the uniform concentration of the remaining liquid, the interface must advance farther when less solute is present.
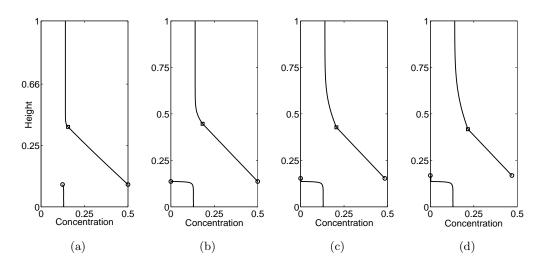
Figure 4.3: Concentration profiles are shown at four different stages of system evolution. The circles in each image represent the location of the solid-mush interface; note the jump in concentration across the interface. The square in each image represents the location of the mush-liquid interface. In (a) we see a sample concentration profile while the eutectic solid-mush front is present. In (b) we see the concentration profile when the transition from eutectic to noneutectic solid-mush interface occurs. Each of (c) and (d) show the concentration profiles at later times, including jumps in the concentration gradient at the mush-liquid interface.

(a)

(b)
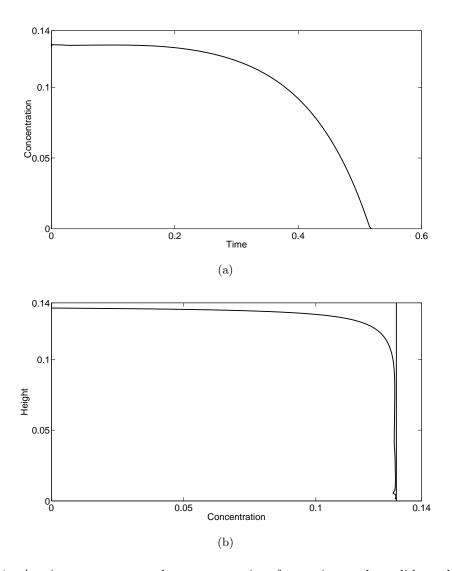
Figure 4.4: As time progresses, the concentration frozen in at the solid-mush interface varies, as demonstrated in (a). We can also see this effect by looking at the concentration profile in the solid when the interface switches from a eutectic interface to a noneutectic interface, as shown in (b). The vertical line in (b) represents the concentration in the solid determined by the semi-infinite domain model.
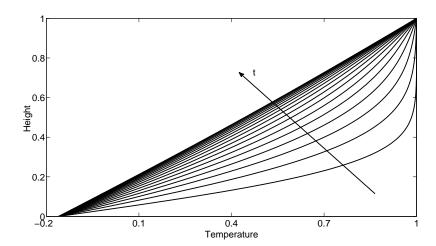
Figure 4.5: Evolution of the temperature profile at evenly space intervals from $t = 0$ until near the steady-state temperature profile.

(a)

(b)
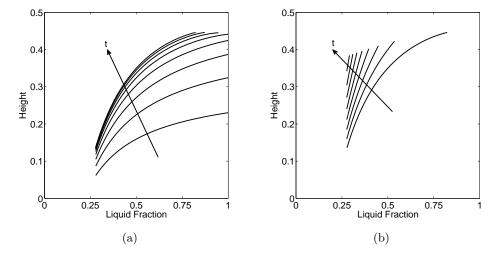
Figure 4.6: The curves are liquid fraction (χ) profiles within the mush at various stages of system evolution. The curves in (a) are at evenly-spaced intervals during the advance of the mush-liquid interface. The remainder of the time until the mush vanishes is illustrated in (b), again at evenly spaced intervals.
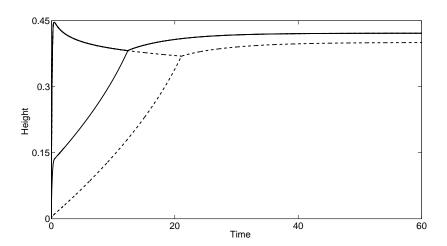
Figure 4.7: The interface positions for the present study (solid curves) are compared with the interface positions ignoring eutectic effects (dashed curves). At early times, both systems have a solid-mush interface (lower curve) and a mush-liquid interface (upper curve), and at later times both systems have a solid-liquid interface. The mushy layer disappears sooner when eutectics are taken into account.

Chapter 5

Conclusions and Future Directions

When a finite-height tank filled with a uniformly-mixed binary alloy is placed onto a cooled boundary, a mushy zone initially advances rapidly from that boundary. As time passes, this advance stops. Eventually, the mush-liquid interface begins to retreat very slowly. There is also a pure solid layer that grows slowly. After a sufficiently large amount of time, the solid-mush interface catches up to the mush-liquid interface, eliminating the mushy layer. After this occurs, the system continues to solidify without a mushy layer until the liquid region homogenizes.

In this dissertation, we have highlighted issues that arise at the solid-mush and mush-liquid interface for the mushy layer problem on a finite domain. A condition of marginal equilibrium is applied at the mush-liquid interface as the free-boundary condition only when the interface is advancing rapidly enough, otherwise the interface is controlled by the diffusion of solute out of the mushy layer and into the liquid layer. The solid-mush interface is initially a eutectic front if the temperature at the base of the tank is sufficiently cold, and later switches to a diffusion-controlled interface. If the temperature at the base of the tank is not as cold, then the diffusion-controlled solid-mush interface appears for all time. Overall, we see that the diffusion of solute is critical in the finite domain case, especially over long timescales, as it drives the advance of the solid-mush interface. These diffusive effects lead to the eventual elimination of the mushy layer.

The differences between the infinite and finite domain cases are fairly significant. For the infinite domain case, the conditions at each interface do not change with time, but instead are dictated by the parameters of the system. In particular, the solid-mush interface is exactly one of either a eutectic front or a diffusion-controlled front for all time. Additionally, if a eutectic front appears, then the concentration of solute in the eutectic solid region is uniform. On the other hand, the interface conditions can change over time for the finite domain. The concentration in the solid can be variable with position, forming three subregions within the solid: a solid region of nearly uniform nonzero concentration at the bottom of the tank, a middle transition region with decreasing concentration, and a pure solid region.

We anticipate that a simple experimental setup could be utilized to validate our results for the noneutectic case. Our parameters roughly approximate a 14% sodium nitrate solution, as described in Set I of Table 1 in Worster (1986), so a tank filled with such a solution at 15 degrees Celsius placed upon a surface cooled to -15.6 degrees Celsius should reflect the results we have provided. The specific results obtained in this study are for a tank that has a height of 15 cm, but a smaller tank would permit an experiment to be completed in

a more reasonable amount of time due to the scaling of time with H^2. For example, a tank with height 3 cm filled with a uniformly mixed 14% sodium nitrate solution is predicted to have no mushy zone remaining after one day. A similar experiment could confirm the effects highlighted for the eutectic case.

An experimental setup for directional solidification has recently been developed, as described in Peppin et al. (2007). Some experimental results obtained with this apparatus have also been described in Peppin et al. (2008). In particular, they show that the mushy layer grows initially, reaches a state which it maintains for some time, and eventually begins to slowly retreat. Such results would seem to highlight the distinction between the finite-size Hele-Shaw cell used in the experiment and the infinite domain used for analytical results. We suspect that our results demonstrate a similar issue, but in a different experimental arrangement.

A number of experiments have been performed with an upper boundary that is insulated, as opposed to an upper boundary fixed at the initial temperature. This change alters the advance of the interfaces, allowing the mush-liquid interface to advance all the way to the upper boundary. Aitta et al. (2001) studied the solidification of a ternary alloy with such an experimental arrangement, and the mush-liquid interface advanced like $h(t) = \alpha t^{1/2}$ over a span of five days. Depending on the temperature at the bottom of the tank, the steady state will either be completely solidified or will have a solid layer and a mushy layer. In an experimental arrangement with an upper boundary cooled below the eutectic temperature and an insulated lower boundary, complete solidification is demonstrated by Kerr et al. (1990c). That study also shows stratification of the composition in the solid phase, which is an effect that we have predicted with both boundaries at fixed temperatures. Appropriate modifications to our model and numerical scheme should be able to capture these effects, where the interfaces advance like $t^{1/2}$ for a longer duration and the possibility of complete solidification.

The work presented in this dissertation provides insights that may allow investigation of a variety of other questions. We will now discuss some of these additional problems.

5.1   Inclusion of latent heat

The assumption of negligible latent heat has been instrumental in the research described in this dissertation. This assumption, combined with the assumption of uniform thermal properties, decoupled the temperature equations from all other quantities in the problem. This then allowed for a straightforward application of the method of characteristics within the mushy layer.

A similar numerical approach to the one presented may be applicable in the presence of latent heat. Such an approach would iterate on the temperature field and both the position of the characteristics and their associated liquid fraction values at the new time step. The liquid fraction at the solid-mush interface will no longer be zero, as this particular condition is a direct result of negligible latent heat. We expect that the behaviors exhibited in the present analysis would still occur. For instance, the steady states when $T_B \geq T_E$ remain unchanged when latent heat is included. Additionally, the mush-liquid interface remains bounded by the isotherm associated with $\theta_L(C_0)$ and the solid-mush interface will slowly advance until the mush vanishes. As previously discussed, varying the Stefan number slows solidification, so the mushy layer may persist longer than predicted here, but it will

ultimately vanish. The overall behavior of the system in the presence of eutectic effects will still be the same, but we would anticipate some small change in the eventual steady state of the system. The quantity of solute being frozen into the solid would likely be reduced, as the advance of the eutectic isotherm would be slowed.

5.2 Nonuniform thermal properties

The assumption of uniform thermal properties played an important role in this research, as it helped to eliminate any dependence of the thermal equations on other quantities in the problem. In a more general setting, the thermal properties in the solid and liquid states are not the same.

For the binary alloy mushy layer problem on an infinite domain, Worster (1986) included nonuniform thermal properties. The thermal properties within the mushy layer varied linearly with the liquid fraction. This introduces a coupling of the equations within the mushy layer. Additionally, as discussed by Worster (1986), the condition of marginal equilibrium may lead to $\chi_{b-} \neq 1$ in this case. For the infinite domain problem, the value of χ_{b-} is uniform in time. On the other hand, for the finite domain problem, the value of χ_{b-} could vary with time, much as can occur at the solid-mush interface in the present study.

5.3 Stability analysis

Much effort has been invested in studying convective instabilities of mushy zones, as can be seen from the review in Worster (1997), along with our discussion in Chapter 1. The results of such investigations should still apply to the present case. For solidification from below, if the rejected component is less dense than the component making up the dendrites, then buoyancy-driven convection is anticipated. In such a case, the long-term behavior demonstrated in this dissertation may be disrupted. If the rejected component has higher density, then convection is not expected.

However, the analysis for the present case will differ from those previous studies. The main difference comes from the fact that the previous studies mainly address the case of directional solidification. In the present case the two interfaces advance at different rates, but the previous studies assume they advance at the same rate. The results presented in Chapters 3 and 4 demonstrate that the similarity solution is a very good approximation to the finite-domain solution at early times, so a stability analysis of the similarity solutions would provide valuable information concerning the early-time stability of the finite domain system. Unfortunately, the similarity solutions do not have a steady state, so the standard techniques do not apply. Additionally, unlike the case of directional solidification, there is no obvious characteristic length scale for the problem.

One approach that provides some insight is that used by Hwang and Choi (2004), who analyzed stability of the system with respect to the similarity solution under the assumptions that no solid layer appears, the base of the tank is at the eutectic temperature, solute diffusion within the mushy layer is negligible, and that the permeability of the mushy layer is uniform. Due to these assumptions, the solid-mush front is pinned to the lower boundary. Their approach assumes periodic perturbations in terms of x and y, but then assumes that the disturbances in z and t are related in terms of the similarity variable. That is, if $\bar{T}(x, y, z, t)$ is the disturbance, then $\bar{T} = \hat{T}(\eta) \exp{(i(\alpha x + \beta y))}$. The mush-liquid interface

is not disturbed, matching the rigid interface assumption used in many of the directional solidification studies.

5.4 Ternary alloys

The infinite domain mushy layer problem with ternary alloys has been addressed in the presence of eutectic effects by Anderson (2003). Ternary alloys impose a number of new complications to the problem. First, the phase diagram is more complex. Second, two different mushy layers form, called the primary and secondary mushy layer. One layer has only one component being solidified with the other two being rejected, and the second has two components being solidified with only one being rejected. Third, due to the presence of three distinct species, one must track the solid fraction due to each component in each region in the domain.

Before the finite domain problem for ternary alloys can be dealt with, the possibility of a diffusion-controlled solid-mush interface must be taken into account. It is quite possible that two such interface could occur, one which rejects two components and one which rejects one component. The dynamics for such interfaces are likely similar to the case for binary alloys, as addressed by Worster (1986).

Overall, we expect that the results of this dissertation would have application to the case of ternary alloys. The disappearance of the mushy layers over time is expected, but the transient behaviors before that point would be of interest. For example, does the secondary mushy layer vanish before the primary mushy layer? Perhaps the answer to that question depends upon the parameters for the system.

Bibliography

Aitta, A., Huppert, H. E., and Worster, M. G. (2001). Diffusion-controlled solidification of a ternary melt from a cooled boundary. *J. Fluid Mech.*, 432:201–217.

Anderson, D. M. (2003). A model for diffusion-controlled solidification of ternary alloys in mushy layers. *J. Fluid Mech.*, 483:165–197.

Aussillous, P., Sederman, A. J., Gladden, L. F., Huppert, H. E., and Worster, M. G. (2006). Magnetic resonance imaging of structure and convection in solidifying mushy layers. *J. Fluid Mech.*, 552:99–125.

Chen, C. F. (1995). Experimental study of convection in a mushy layer during directional solidification. *J. Fluid Mech.*, 293:81–98.

Chen, C. F. and Chen, F. (1991). Experimental study of directional solidification of aqueous ammonium-chloride solution. *J. Fluid Mech.*, 227:567–586.

Chung, C. A. and Chen, F. L. (2000). Onset of plume convection in mushy layers. *J. Fluid Mech.*, 408:53–82.

Davis, S. H. (2001). *Theory of Solidification*. Cambridge University Press.

Emms, P. W. and Fowler, A. C. (1994). Compositional convection in the solidification of binary alloys. *J. Fluid Mech.*, 262:111–139.

Evans, L. C. (1998). *Partial Differential Equations*. American Mathematical Society.

Fowler, A. C. (1985). The formation of freckles in binary alloys. *IMA J. Appl. Math.*, 35:159–174.

Gewecke, N. R. and Schulze, T. P. (2011). The rapid advance and slow retreat of a mushy zone. *J. Fluid Mech.*, doi:10.1017/S0022112011000103.

Hills, R. N., Loper, D. E., and Roberts, P. H. (1983). A thermodynamically consistent model of a mushy zone. *Q. J. Appl. Math.*, 36:505–539.

Huppert, H. E. and Worster, M. G. (1985). Dynamic solidification of a binary melt. *Nature*, 314:703–707.

Hwang, I. G. and Choi, C. K. (2004). Onset of compositional convection during solidification of a two-component melt from a bottom boundary. *J. Cryst. Growth*, 267:714–723.

Kerr, R. C., Woods, A. W., Worster, M. G., and Huppert, H. E. (1990a). Solidification of an alloy cooled from above. part 1. equilibrium growth. *J. Fluid Mech.*, 216:323–342.

Kerr, R. C., Woods, A. W., Worster, M. G., and Huppert, H. E. (1990b). Solidification of an alloy cooled from above. part 2. non-equilibrium interfacial kinetics. *J. Fluid Mech.*, 217:331–348.

Kerr, R. C., Woods, A. W., Worster, M. G., and Huppert, H. E. (1990c). Solidification of an alloy cooled from above. part 3. compositional stratification within the solid. *J. Fluid Mech.*, 218:337–354.

Langer, J. (1980). Instabilities and pattern formation in crystal growth. *Reviews of Modern Physics*, 52:1–28.

Le Bars, M. and Worster, M. G. (2006). Solidification of a binary alloy: Finite-element, single-domain simulation and new benchmark solutions. *J. Comput. Phys.*, 216:247–263.

Mullins, W. W. and Sekerka, R. F. (1964). Stability of a planar interface during solidification of a dilute binary alloy. *J. Appl. Phys.*, 35:444–451.

Notz, D., Wettlaufer, J. S., and Worster, M. G. (2005). A non-destructive method for measuring the salinity and solid fraction of growin sea ice in situ. *J. Glaciol.*, 51:159–166.

Peppin, S. S. L., Aussillous, P., Huppert, H. E., and Worster, M. G. (2007). Steady-state mushy layers: experiments and theory. *J. Fluid Mech.*, 570:69–77.

Peppin, S. S. L., Huppert, H. E., and Worster, M. G. (2008). Steady-state solidification of aqueous ammonium chloride. *J. Fluid Mech.*, 599:465–476.

Roper, S. M., Davis, S. H., and Voorhees, P. W. (2007). Convection in a mushy zone forced by sidewall heat losses. *Metall. Mater. Trans. A*, 38:1069–1079.

Roper, S. M., Davis, S. H., and Voorhees, P. W. (2008). An analysis of convection in a mushy layer with a deformable permeable interface. *J. Fluid Mech.*, 596:333–352.

Rutter, J. W. and Chalmers, B. (1953). A prismatic substructure formed during solidification of metals. *Can. J. Phys.*, 31:15–39.

Sample, A. K. and Hellawell, A. (1984). The mechanisms of formation and prevention of channel segregation during alloy solidification. *Metall. Trans. A*, 15:2163–2173.

Schulze, T. P. and Worster, M. G. (1999). Weak convection, liquid inclusions and the formation of chimneys in mushy layers. *J. Fluid Mech.*, 388:197–215.

Schulze, T. P. and Worster, M. G. (2005). A time-dependent formulation of the mushy-zone free-boundary problem. *J. Fluid Mech.*, 541:193–202.

Shirtcliffe, T. G. L., Huppert, H. E., and Worster, M. G. (1991). Measurement of the solid fraction in the crystallization of a binary melt. *J. Cryst. Growth*, 113:566–574.

Shirtcliffe, T. G. L. and Kerr, R. C. (1992). On the use of electrical resistance and temperature as measures of the solid fraction in a mushy layer. *J. Cryst. Growth*, 125:495–501.

Solomon, T. H. and Hartley, R. R. (1998). Measurements of the temperature field of mushy and liquid regions during solidification of aqueous ammonium chloride. *J. Fluid Mech.*, 358:87–106.

Wettlaufer, J. S., Worster, M. G., and Huppert, H. E. (1997a). Natural convection during solidification of an alloy from above with application to the evolution of sea ice. *J. Fluid Mech.*, 344:291–316.

Wettlaufer, J. S., Worster, M. G., and Huppert, H. E. (1997b). The phase evolution of young sea ice. *Geophys. Res. Lett.*, 24:1251–1254.

Wilson, D., Solomon, A. D., and Alexiades, V. (1984). A model of binary alloy solidification. *Int. J. Numer. Meth. Eng.*, 20:1067–1084.

Wilson, D. G., Solomon, A. D., and Alexiades, V. (1982). A shortcoming of the explicit solution for the binary alloy solidification problem. *Lett. Heat Mass Trans.*, 9:421–428.

Worster, M. G. (1986). Solidification of an alloy from a cooled boundary. *J. Fluid Mech.*, 167:481–501.

Worster, M. G. (1992). Instabilities of the liquid and mushy regions during solidification of alloys. *J. Fluid Mech.*, 237:649–669.

Worster, M. G. (1997). Convection in mushy layers. *Annu. Rev. Fluid Mech.*, 29:91–122.

Worster, M. G. and Wettlaufer, J. S. (1997). Natural convection, solute trapping, and channel formation during solidification of saltwater. *J. Phys. Chem. B*, 101:6132–6136.

Appendices

Appendix A

Liquid fraction at the similarity solution solid-mush interface

We have claimed that the liquid fraction at the solid-mush interface is zero for the similarity solution discussed in Worster (1986) under the assumptions of negligible latent heat and uniform thermal properties, for $T_B \geq T_E$. Also, the numerical scheme incorporates the similarity solution at the initial time, so the liquid fraction at that interface needs to be known. The differential equation governing the liquid fraction in the mush, in terms of the similarity variable, develops a singularity under the present assumptions. This disrupts numerical integration of the similarity solution. However, as we will demonstrate, we can analytically derive that the similarity solution has zero liquid fraction at the solid-mush interface.

The system for the similarity solution is similar to the system presented in this paper. However, since the similarity solution uses an infinite domain, the conditions that we use at $z = 1$ for the finite domain are replaced with the farfield ($z \to \infty$) conditions,

$$\theta \to 1, \ C \to C_0.$$

As in the finite-domain case, the temperature field decouples from the rest of the system under our assumptions. In this case, the temperature field is given by

$$\theta(z, t) = \mathrm{erf}\left(\frac{z}{2\sqrt{t}}\right),$$

where the error function $\mathrm{erf}(x)$ is defined to be

$$\mathrm{erf}(x) = \frac{2}{\sqrt{\pi}} \int_0^x \exp(\psi^2) \, d\psi.$$

Equivalently, this is

$$\theta(\eta) = \mathrm{erf}(\eta),$$

where

$$\eta = \frac{z}{2\sqrt{t}},$$

is a similarity variable. Under this similarity transformation, the equation governing the

liquid fraction in the mush becomes

$$\left(2\eta C + \epsilon C'\right)\chi' = -\left(2\eta C' + \epsilon C''\right)\chi. \tag{A.1}$$

Furthermore, due to the liquidus relationship, the concentration and its derivatives in the mush are given by

$$C(\eta) = C_B - \frac{1}{\hat{\Gamma}}\mathrm{erf}(\eta),$$

$$C'(\eta) = -\frac{2}{\hat{\Gamma}\sqrt{\pi}}\exp\left(-\eta^2\right),$$

$$C''(\eta) = \frac{4\eta}{\hat{\Gamma}\sqrt{\pi}}\exp\left(-\eta^2\right).$$

We can solve for the concentration C_b at the mush-liquid interface $\eta = \lambda_b$ (see Worster (1986) for details), and as a result we can integrate (A.1) to solve for the liquid fraction throughout the mush,

$$\chi(\eta) = \chi_b \exp\left(\int_\eta^{\lambda_b} \frac{\left(2\xi C'(\xi) + \epsilon C''(\xi)\right)}{2\xi C(\xi) + \epsilon C'(\xi)}\, d\xi\right).$$

Due to the condition of marginal equilibrium in the special case of uniform thermal properties in all phases, we have that $\chi_b = 1$, so

$$\chi(\eta) = \exp\left(\int_\eta^{\lambda_b} \frac{\left(2\xi C'(\xi) + \epsilon C''(\xi)\right)}{2\xi C(\xi) + \epsilon C'(\xi)}\, d\xi\right).$$

The free-interface condition for the solid-mush interface (2.13c) transforms to

$$\left(2C_a\lambda_a + \epsilon C_a'\right)\chi_a = 0,$$

where $\eta = \lambda_a$ denotes the interface position in terms of the similarity variable. This requires either $\chi_a = 0$ or $2\lambda_a C_a + \epsilon C_a' = 0$. In the latter case, we will show that the interface is located at a regular singular point of (A.1).

Equation (A.1) admits $\chi = 0$ as a solution everywhere. However, this is inconsistent with $\chi_b = 1$, so we need to focus our attention to the behavior of the solution near the singularity. We can rewrite (A.1) as

$$\chi' + \frac{2\eta C' + \epsilon C''}{2\eta C + \epsilon C'}\chi = 0.$$

If we can show that the function

$$p(\eta) = \frac{2\eta C' + \epsilon C''}{2\eta C + \epsilon C'},$$

has a simple pole at the singularity, that is when $2\eta C + \epsilon C' = 0$, then we can examine the series solution to determine the behavior of the solution near the singularity. We denote the location of the singularity as ξ_s.

Consider the function $f(\eta) = 2\eta C + \epsilon C'$. We have already solved for $C(\eta)$ and $C'(\eta)$, so

$$f(\eta) = 2\eta C_B - \frac{2\eta}{\hat{\Gamma}}\text{erf}(\eta) - \frac{2\epsilon}{\hat{\Gamma}\sqrt{\pi}}\exp(-\eta^2).$$

If we can show that $f'(\xi_s) \neq 0$, then $p(\eta)$ has a simple pole at $\eta = \xi_s$. Now,

$$f'(\eta) = 2C_B - \frac{2}{\hat{\Gamma}}\left[\text{erf}(\eta) + \frac{2(1-\epsilon)\eta}{\sqrt{\pi}}\exp\left(-\eta^2\right)\right],$$

which is zero only if the bracketed expression is equal to $\hat{\Gamma}C_B$. We will now focus our attention on the bracketed expression, which we will now call $g(\eta)$. First, we note that $g(0) = 0$. Then, we see that

$$g'(\eta) = \frac{-2}{\sqrt{\pi}}\exp\left(-\eta^2\right)[\epsilon + (1-\epsilon)\eta],$$

which is negative for all $\eta \geq 0$. As a result, $g(\eta) \leq 0$ for all $\eta \geq 0$, so $g(\eta) \neq \hat{\Gamma}C_B$ for any $\eta \geq 0$.

From the above, we see that $f'(\eta) \neq 0$ for $\eta \geq 0$, so $f(\xi_s) \neq 0$. Therefore, $p(\eta)$ has a simple pole at $\eta = \xi_s$. There exists a regular series solution to (A.1) near $\eta = \xi_s$ of the form

$$\chi(\eta) = \sum_{n=0}^{\infty} a_n (\eta - \xi_s)^{n+r},$$

with

$$r = -\lim_{\eta\to\xi_s}(\eta - \xi_s)p(\eta) = \frac{-2(1-\epsilon)\xi_s^2}{2(1-\epsilon)\xi_s^2 - \epsilon}.$$

For the parameters described in the main text of the paper, we have $r \approx 0.011$.

From the above, we see that

$$\lim_{\eta\to\xi_s^+}\chi(\eta) = 0,$$

so we conclude that $\lambda_a = \xi_s$, and that both conditions $\chi_a = 0$ and $2\lambda_a C_a + \epsilon C_a' = 0$ are satisfied at the interface. Furthermore, the series solution above indicates very rapid growth of the liquid fraction near the solid-mush interface.

Vita

Nicholas Ray Gewecke was born, along with his twin brother Heath, in Lincoln, Nebraska, on June 22, 1983, to Allen and Nancy Gewecke. He grew up in Lincoln, graduating from Lincoln High School in 2001. That same year, he proceeded to enroll at the University of Nebraska - Lincoln, where he earned a Bachelor of Science in Mathematics, with minors in Physics and Spanish. After graduating in 2005, he moved to Knoxville, Tennessee, to attend the University of Tennessee - Knoxville and pursue a Ph.D. in Mathematics.